ISSN 2472-1972

In Vitro Impact of FSH Glycosylation Variants on FSH Receptor-stimulated Signal Transduction and Functional Selectivity

Teresa Zariñán,[1] Viktor Y. Butnev,[2] Rubén Gutiérrez-Sagal,[1] José Luis Maravillas-Montero,[1] Iván Martínez-Luis,[1] Nancy R. Mejía-Domínguez,[1] Guillermo Juárez-Vega,[1] George R. Bousfield,[2] and Alfredo Ulloa-Aguirre,[1]

[1]Red de Apoyo a la Investigación (RAI), Universidad Nacional Autónoma de México (UNAM)-Instituto Nacional de Ciencias Médicas y Nutrición Salvador Zubirán, Mexico City 14000, Mexico; and [2]Department of Biological Sciences, Wichita State University, Wichita, Kansas 67260, USA

ORCiD numbers: 0000-0002-9532-3886 (A. Ulloa-Aguirre).

FSH exists as different glycoforms that differ in glycosylation of the hormone-specific β-subunit. Tetra-glycosylated FSH (FSH^{24}) and hypo-glycosylated FSH ($FSH^{18/21}$) are the most abundant glycoforms found in humans. Employing distinct readouts in HEK293 cells expressing the FSH receptor, we compared signaling triggered by human pituitary FSH preparations ($FSH^{18/21}$ and FSH^{24}) as well as by equine FSH (*e*FSH), and human recombinant FSH (*rec*FSH), each exhibiting distinct glycosylation patterns. The potency in eliciting cAMP production was greater for *e*FSH than for $FSH^{18/21}$, FSH^{24}, and *rec*FSH, whereas in the ERK1/2 activation readout, potency was highest for $FSH^{18/21}$ followed by *e*FSH, *rec*FSH, and FSH^{24}. In β-arrestin1/2 CRISPR/Cas9 HEK293-KO cells, $FSH^{18/21}$ exhibited a preference toward β-arrestin-mediated ERK1/2 activation as revealed by a drastic decrease in pERK during the first 15-minute exposure to this glycoform. Exposure of β-arrestin1/2 KO cells to H89 additionally decreased pERK1/2, albeit to a significantly lower extent in response to $FSH^{18/21}$. Concurrent silencing of β-arrestin and PKA signaling, incompletely suppressed pERK response to FSH glycoforms, suggesting that pathways other than those dependent on Gs-protein and β-arrestins also contribute to FSH-stimulated pERK1/2. All FSH glycoforms stimulated intracellular Ca^{2+} (iCa^{2+}) accumulation through both influx from Ca^{2+} channels and release from intracellular stores; however, iCa^{2+} in response to $FSH^{18/21}$ depended more on the latter, suggesting differences in mechanisms through which glycoforms promote iCa^{2+} accumulation. These data indicate that FSH glycosylation plays an important role in defining not only the intensity but also the functional selectivity for the mechanisms leading to activation of distinct signaling cascades.

Key Words: follicle-stimulating hormone, follicle-stimulating hormone receptor, macroheterogeneity, glycosylation, signal transduction, functional selectivity, biased agonism

FSH, or follitropin, is synthesized and secreted by the anterior pituitary gland in multiple molecular forms that vary in oligosaccharide number and type of carbohydrate moieties attached to the protein core [1, 2]. This gonadotropin is composed of 2 subunits associated through noncovalent interactions: an α-subunit, which is common to all glycoprotein

Abbreviations: AUC, area under the curve; eFSH, equine FSH; Emax, dose necessary to reach maximal cAMP production; FSHR, FSH receptor; hFSH, human FSH; hFSHR, human RSH receptor; IBMX, 3-isobutyl-methyl-xantine; iCa2+, intracellular Ca2+; KD, equilibrium dissociation constant; MAb, monoclonal antibody; PMSF, phenylmethanesulfonyl fluoride; recFSH, recombinant FSH; WB, Western blot

Received 27 November 2019
Accepted 14 February 2020
First Published Online 18 February 2020
Corrected and Typeset 21 April 2020

hormones (LH, chorionic gonadotropin, and TSH) and a FSHβ-subunit, which confers specificity to the gonadotropin [3]. In the human FSH (hFSH) heterodimer, 4 Asn residues, αN52, αN78, βN7, and βN24 are targets for N-linked glycosylation (Fig. 1) [4]. Oligosaccharide heterogeneity in glycoprotein hormones comes in 2 forms, macroheterogeneity, which results from the absence of 1 or more oligosaccharide chains from a hormone variant [5–8], and microheterogeneity resulting from variations in the type of carbohydrates comprising the oligosaccharide populations attached to the protein core of the hormone [9–14]. In general, oligosaccharides on the β-subunit play a major role in determining the circulatory half-life

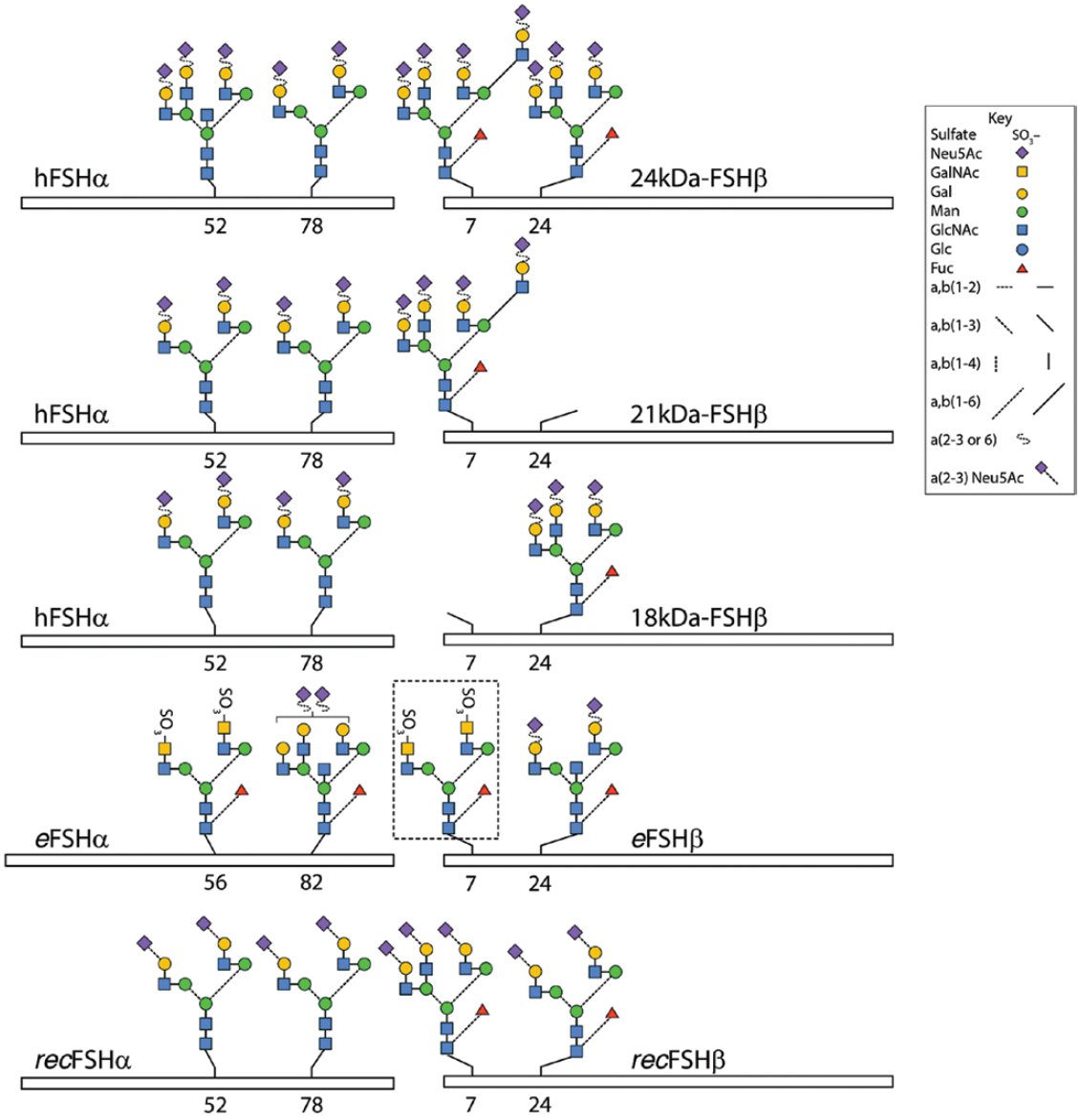

Figure 1. Typical glycans attached to human pituitary FSH, human recombinant FSH produced by Chinese hamster ovary cells (*rec*FSH) glycoforms, and equine FSH (*e*FSH). The bars indicate the common-α and hormone-specific FSHβ subunits. N-glycosylation sites are indicated by the numbers below the bars. The *e*FSHα subunit has 4 additional residues at the N-terminus, accounting for the difference in numbering. The glycan at position β7 in *e*FSH (dotted area) is absent from 90% of the molecules present in highly purified preparations [34]. Glycans attached to *rec*FSH were taken from the report by Mastrangeli et al [104]. Note that glycans at the α subunit of $FSH^{18/21}$ are in fact smaller (*i.e.* biantennary) than those present in FSH^{24}, which account for the different migration profiles of $FSH^{18/21}$ shown in Fig. 2D.

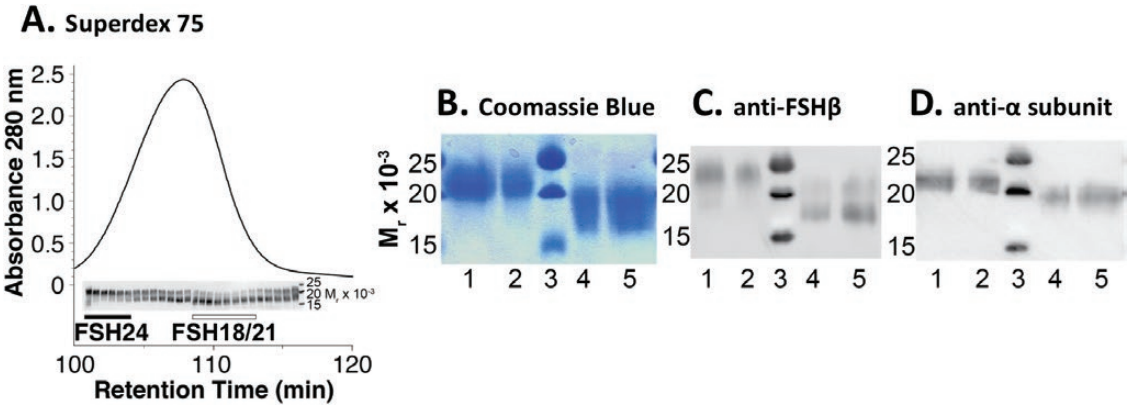

Figure 2. (A) Superdex 75 chromatography of immunopurified pituitary hFSH. Three 1 × 30 cm Superdex 75 columns were connected in series and equilibrated with 0.2 M ammonium bicarbonate containing 20% acetonitrile. The chromatogram was developed with the same buffer using a flow rate of 0.4 mL/min at 25°C. Fractions under the FSH heterodimer peak were collected and 1-µg samples evaluated by Western blot using anti-FSHβ antibody 15-1.E3.E5 [45] diluted 1:2000 (inset). The solid bar indicates fractions pooled to obtain FSH^{24} and the open bar indicates fractions pooled to obtain $FSH^{18/21}$. (B-D) FSH glycoform preparations. Samples of FSH^{24} (VB-II-277A) and $FSH^{18/21}$ (VB-II-277B) were subjected to SDS-PAGE under reducing conditions and FSH was detected by (B) Coomassie Blue staining, (C) FSHβ Western blot, or (D) FSHα Western blot. (B) Lane 1, 5 µg FSH^{24}; lane 2, 2.5 µg FSH^{24}; lane 3, BioRad Precision Plus MW markers; lane 4, 2.5 µg $FSH^{18/21}$; lane 5, 5 µg $FSH^{18/21}$. (C,D) Western blots with anti-FSHβ antibody 15-1.E3.E5 [45] diluted 1:2000 and anti-FSHα antibody 15-2.C3.C5 [36, 105] diluted 1:1000, respectively. Lane 1, 1 µg FSH^{24}; lane 2, 0.5 µg FSH^{24}; lane 3, BioRad Precision Plus MW markers; lane 4, 0.5 µg $FSH^{18/21}$; lane 5, 1 µg $FSH^{18/21}$. Differences in migration between the α-subunits of FSH^{24} (lanes 1 and 2) and $FSH^{18/21}$ (lanes 4 and 5) in panel D are due to the higher content of smaller, biantennary glycans at both Asn^{52} and Asn^{78} in the latter, which led to a more rapid migration in the blot.

and in vivo bioactivity of the gonadotropin [15], whereas the oligosaccharide in position αAsn^{52} is primarily involved in activation of the receptor/signal transducer (G protein) system and the ensuing biological response [16–19], an effect probably mediated through stabilizing the structure and/or conformation of the hFSH dimer particularly upon binding to its cognate receptor [20–22]. Nevertheless, previous and more recent studies have shown that glycans at αAsn^{78} and oligosaccharides in the β-subunit also play an important role in hFSH-mediated signal transduction [23–26].

hFSH macroheterogeneity occurs at either 1 or both FSHβ N-glycosylation sites [5–7] (Fig. 1). Western blots of hFSH revealed the presence of 2 FSHβ bands, a 24-kDa band that possesses both Asn^{7} and Asn^{24} N-linked glycans (designated as fully/tetra-glycosylated, 24 kDa-FSHβ) and a 21-kDa band that lacks the Asn^{24} glycan (hypo-glycosylated, 21 kDa-FSHβ) [5, 8]. The corresponding hFSH heterodimers are designated FSH^{24} and FSH^{21}, respectively. Purified FSH^{21} preparations include a second hypo-glycosylated variant, 18 kDa-FSHβ, which lacks the Asn^{7} glycan. The corresponding heterodimer is designated as FSH^{18}. In addition, both αFSH^{21} and αFSH^{18} bear more biantennary glycans than FSH^{24}. A third hypo-glycosylated 15 kDa-FSHβ variant has been isolated from human pituitaries; however, studies in transgenic mice indicate poor assembly with FSHα and very low levels of secretion of the FSH^{15} glycoform [27]. Thus, there appear to be 3 physiologically relevant hFSH variants, FSH^{24}, FSH^{21}, and FSH^{18}.

In vitro and in vivo studies have shown that naturally occurring pituitary- and GH3 cell-derived recombinant hFSH glycoforms exhibit distinct FSH receptor (FSHR) binding kinetics and bioactivity as compared to fully glycosylated hFSH [25, 26, 28, 29]. Thus, similar to the influence of microheterogeneity on the ability of the gonadotropins to activate and trigger intracellular signaling [12, 13, 30], FSHβ macroheterogeneity may also contribute to its bioactivity.

It is currently accepted that in many cell systems FSH stimulation triggers activation of a complex array of nonlinear signaling cascades mediated not only by the canonical Gs/cAMP/protein kinase A pathway but also by other G proteins and FSHR receptor interacting proteins [31, 32]. Considering that activation of this complex signaling network and, in particular, of distinct signaling modules probably occurs through stabilization of distinct FSHR conformations in response to binding of particular ligands [29], we here analyzed the in vitro functional effects of several tetra- and hypo-glycosylated FSH glycoforms employing multiple readouts to facilitate identification of glycosylation-promoted preferential activation of one or more signaling pathways in the same ligand/receptor system (i.e., biased agonism [33]) among the different FSH glycoforms. For this purpose, we analyzed the effects of four distinct highly purified FSH preparations, tetra- and hypo-glycosylated pituitary hFSH (FSH^{24} and $FSH^{18}/^{21}$, respectively), equine FSH (*e*FSH, 90% hypo-glycosylated (Fig. 1) [34]), and Chinese-hamster ovary cell-produced human recombinant FSH (*rec*FSH or follitropin-α; tetra-glycosylated), using cultured human embryonic kidney-293 (HEK293) cells stably expressing the human FSHR (hFSHR) as the target for FSH action. These four preparations also differ, to varying extents, in microheterogeneity, including differences in oligosaccharide complexity determined by the number of antennas attached to the N-linked oligosaccharide core, degree of sialylation, fucosylation and sulfation, position of terminal sialic acid residues (α2-6-linked, α2-3-linked, or both), and presence of bisecting GlcNAc residues (Fig. 1) [5, 34–43].

1. Material and Methods

A. Hormones

Human pituitary FSH glycoforms were purified from lyophilized pituitary tissue (a generous gift of Dr. James A. Dias, The University at Albany, Albany, NY). *e*FSH (batch VB-I-171) was purified from horse pituitaries obtained from Animal Technologies, Inc., (Tyler, TX). Recombinant human FSH produced in Chinese hamster ovary cells (batches AU012310 and BA024393) was a kind gift of Merck Serono (Mexico City, Mexico); according to the manufacturer, the reported batch-to-batch consistency for this particular preparation is relatively high as disclosed by the coefficients of variation in the range of 7% to 15% for the most and least abundant isoforms of the gonadotropin [38].

B. Human FSH Glycoform and eFSH Purification

A 600-g batch of lyophilized human pituitaries was homogenized using 3, 15-second bursts at a setting of 10 with a Brinkman PT-10 Polytron in water containing 1 mM phenylmethanesulfonyl fluoride (PMSF) at 4°C. The extract was adjusted to pH 5.5 with HCl and extraction continued for a total of 15 minutes [44]. The extract was centrifuged for 30 minutes at 30,000 × *g* at 4°C, the supernatant was decanted, its volume measured, and adjusted to 75% saturated ammonium sulfate. After overnight precipitation, centrifugation, dialysis, and lyophilization, the dried protein was fractionated on a 5.0 cm × 200 cm Sephacryl S-100 column in 0.126 M ammonium bicarbonate buffer, pH 7.8. The column fractions were tested for hFSH by radioimmunoassay using reagents obtained from the National Hormone and Pituitary Program, and immunopositive fractions were pooled and lyophilized. hFSH was immunopurified from this fraction by 4 rounds of immunoaffinity chromatography using 2 anti-human FSHβ monoclonal antibody (MAb) columns, 1 prepared with mAb 15-1.E3.E5 [45] (a mouse monoclonal recognizing the FSHβ subunit that is influenced by N-glycosylation) produced in our laboratory, and another with mAb 4882 [46] (mouse monoclonal raised against hFSH recognizing FSH via the α-subunit)] (a generous gift of SP Development Co., Ltd, Bedford, UK), connected in series [36]. The hFSH preparations recovered after 4 cycles of affinity chromatography were combined and fractionated on 3, 1 × 30 cm Superdex 75 columns (GE Healthcare Life Sciences,

Marlborough, MA) connected in series, to separate FSH^{24} and $FSH^{18/21}$ glycoforms as previously described [36]. All Superdex 75 fractions were characterized separately. Glycoform abundance in each fraction was determined by Western blot analysis using anti-human FSHβ monoclonal antibody 15-1.E3.E5 [45]. The fractions possessing largely 24 kDa-FSHβ were pooled to generate FSH^{24} and those possessing largely 18kDa- and 21 kDa-FSHβ were pooled to obtain $FSH^{18/21}$.

*e*FSH was purified by our previously reported method, modified by 75% ammonium sulfate precipitation of the 50% ethanol extract before CM-Sephadex ion exchange chromatography [47].

C. Cell Culture

Authenticated human embryonic 293 kidney (HEK293) cells stably expressing the recombinant hFSHR (HEK293-$hFSHR^+$) driven by the cytomegalovirus promoter [48], with less than 5 consecutive passages, were maintained in a humidified atmosphere of 5% CO_2 at 37°C in high-glucose DMEM (Life Technologies Inc., Grand Island, NY) supplemented with 10% fetal calf serum (Sigma Aldrich, St. Louis, MO), 5 μg/mL geneticin (Life Technologies), and antibiotic (penicillin plus streptomycin) reagent (Life Technologies). Expression of the hFSHR protein at the cell surface plasma membrane was verified by immunoblotting as described later. Cells were grown to 70% to 80% confluence in 100-mm-diameter cell culture dishes (Corning, Corning, NY) at 37°C and an initial density of 1×10^6 cells. Twenty-four hours before the experiment, cells were mechanically dispersed and plated at a density of 75 or 200×10^3 cells/500 μL in 12- or 24-well culture dishes (Corning), depending on the particular experiment (see the following section). On the day of the experiment, cells were starved for 4 hours in DMEM-HEPES 10 mM medium (Life Technologies) supplemented with antibiotic and 0.1% BSA (Sigma). All experiments were performed in triplicate incubations, unless specified, and repeated at least 3 times.

2. Surface Plasmon Resonance

A. Membrane Preparation and Biacore Kinetic Analysis

Cultured HEK293-$hFSHR^+$ cells were collected from confluent 100 × 15 mm culture dishes (Corning). Cells were centrifuged twice at 1000 × *g* for 10 minutes with PBS to finally obtain a pellet that was resuspended in 1 mL ice-cold 20 mM Tris-HCl, pH 8.0, 1 mM EDTA, 1 mM EGTA, 0.1 mM PMSF, 2 mg/mL aprotinin, and 10 mg/mL leupeptin homogenization solution. Cells were then lysed with 10 strokes in a Dounce homogenizer, and then centrifuged at 30,000 × *g* for 20 minutes. The pellet was redissolved in 1 mL of 20 mM Tris-HCl, pH 8.0, 3 mM MgCl, 10 mg/mL DNAase I plus PMSF, 2 mg/mL aprotinin, and 10 mg/mL leupeptin resuspension solution (Sigma), and homogenized again. A final centrifugation at 30,000 × *g* for 20 minutes was performed and the pellet containing the membrane fraction was redissolved in 0.5 mL of resuspending solution, homogenized, and stored at 4°C for immediate use.

Surface plasmon resonance was performed using the Biacore system (Biacore T200, GE Healthcare Life Sciences). The capture surface was prepared to achieve a target immobilization level of 10,000 RU with the membrane fraction preparation. Conditioning and baseline stabilization were accomplished with a short pulse of NaOH (10 mM) injected at a flow rate of 10 μL/min for 60 seconds before BSA (0.1 mg/mL) was injected during 1 minute to ensure complete blocking of nonspecific binding sites. Surface regeneration was accomplished using a 2-step process: 15 seconds of HBS-N (0.1 M HEPES, 1.5 M NaCl) at 20 μL/min for 60 seconds, followed by 2 injections of OGP 40 mM (Octyl β-D glucopyranoside) detergent solution at 10 μL/min for 60 seconds. Measurement of the equilibrium dissociation constant (KD) was performed at 25°C in HBS-EN buffer. Binding curves were generated in duplicate by injecting the hFSH glycoforms for 120-second association followed by 600-second

dissociation at 30 μL/min in individual runs. Kinetic coefficients were calculated with the Biacore T200 Evaluation software using the 1:1 Langmuir binding model with global fit parameters and the bulk refractive index value held constant at zero [49]. Based on the dissociation rate constant (K_d) (s − 1) and association rate constant (K_a) (M^{-1} s^{-1}) obtained, the equilibrium dissociation or affinity constant KD (M) was calculated as the ratio of the rate constant k_a and k_d ($KD = k_d / k_a$).

B. cAMP Production

HEK293-hFSHR$^+$ cells cultured in 24-well plates at a density of 75×10^3 cells/500 μL, were starved for 4 hours and then stimulated with increasing doses (0 to 150 ng/mL of FSH dissolved in DMEM) of each FSH glycoform preparation ($FSH^{18/21}$, FSH^{24}, *e*FSH, and *rec*FSH) in DMEM supplemented with 0.125 mM 3-isobutyl-methyl-xantine (IBMX) (Sigma). At the end of the 3-hour incubation period, cells and media were removed from triplicate wells and total (extra- plus intracellular) cAMP accumulation was measured in acetylated samples by radioimmunoassay as described previously [50], using 2-O-monosuccinyl cAMP tyrosyl methyl ester iodinated by the chloramine T method as the labeled ligand and the CV-125 anti-cAMP antibody [51] (provided by Dr. Albert Parlow and the National Hormone and Peptide Program, Harbor-UCLA Medical Center, Los Angeles, CA) at a 1:70,000 final dilution. For the kinetics of cAMP production, cells were exposed to 50 ng/mL of FSH^{24}, $FSH^{18/21}$, and *e*FSH, or 100 ng/mL *rec*FSH (which corresponds to the dose necessary to reach maximal cAMP production [E_{max}] for cAMP production of each glycoform; see Results) during 0 to 120 minutes. At each time period (every 5 minutes for the first 20 minutes and then every 10 minutes during the ensuing 100 minutes) during the incubation time, cells and media were collected and submitted to total cAMP measurement as described previously.

C. Reporter Gene Assay

For the reporter gene assay, cultured HEK293-hFSHR$^+$ cells (75×10^3 cells/500 μL) were transiently transfected with the cAMP-sensitive pSOMLuc reporter plasmid (kindly donated by Dr. Eric Reiter, Institut National de la Recherche Agronomique, Nouzilly, France) using a previously described procedure [52]. After a 6-hour incubation period in the presence or absence of increasing doses (0–100 ng/mL) of each FSH glycoform preparation dissolved in equal volumes of DMEM, cells were lysed and luciferase activity measured using a luciferase assay system (Promega Co., Madison, WI). The light produced was measured in a luminescence counter and expressed as fold increase over basal.

D. Western Blots of the hFSHR and β-arrestins 1 and 2

After sodium dodecyl sulfate polyacrylamide gel electrophoresis (SDS-PAGE) (7.5%), Western blotting of whole cell lysates from HEK293-hFSHR$^+$ cells was performed using as primary antibody the highly specific anti-human FSHR monoclonal antibody mAb106.105 [53, 54] (kindly donated by Dr. James A. Dias, University at Albany, Albany, NY) and the secondary anti-mouse IgG horseradish peroxidase conjugate (Jackson ImmunoResearch Laboratories Inc, West Grove, PA) [55], as previously described [56]. Development of the signal was performed using the Clarity Western ECL substrate kit (BIORAD, Hercules, CA). A reprobed membrane with a 1:3000 anti-mouse glyceraldehyde-3-phosphate dehydrogenase monoclonal antibody (Merck Millipore, Burlington, MA) [57] and 1:10,000 goat-anti-mouse IgG conjugated with horseradish peroxidase (Jackson ImmunoResearch) [55] was used to confirm equal protein gel loading.

Western blotting of β-arrestins 1 and 2 (β-arr1/2) was performed in cell lysates from control and CRISPR β-arr1/2 HEK293-hFSHR$^+$ KO cells. After SDS-PAGE (10%), blocked membranes were probed with the monoclonal anti-β-arrestin 1 antibody D803J [58] or with anti-β-arrestin 2 antibody C16D9 [59](Cell Signaling Technology, Danvers, MA) at a 1:3000

dilution, and then with donkey anti-rabbit IgG-horseradish peroxidase conjugate (GE Healthcare Life Sciences, Chicago, IL) [60] at a 1:4500 dilution. Development of the signal and verification of protein gel loading were performed as above.

E. ERK1/2 Phosphorylation

HEK293-FSHR$^+$ cells were replated at a density of 200,000 cells/500 μL in 12-well culture plates (Corning) and tested for FSH-stimulated ERK1/2 phosphorylation [52, 61, 62]. Briefly, after a 4-hour preincubation period in serum-free medium (DMEM-10 mM HEPES plus 0.1% BSA and 100 IU/mL penicillin-streptomycin reagent), 0 to 300 ng/mL or 50 ng of each FSH glycoform were added to cells and incubated for 5 or 120 minutes. At the end of the incubation period, cells were lysed in 2X Laemmli buffer and analyzed by Western blot (WB). The membranes were incubated overnight at 4°C with rabbit anti-human phospho-ERK1/2 (1:3000) antibody (Cell Signaling) [63] and then with secondary anti-rabbit IgG horseradish peroxidase conjugate (GE Healthcare) [60]. Equal protein loading was confirmed in a membrane reprobed with primary polyclonal antibody against total ERK1/2 (1:10,000) (Santa Cruz Biotechnology Inc., Santa Cruz, CA) [64]. Development of the signal was performed using the Clarity Western ECL substrate kit (BIORAD). In a second set of studies, HEK293-hFSHR$^+$ control cells and CRISPR β-arr1/2 HEK293-hFSHR$^+$ KO cells (see the following section), were incubated with 50 ng/mL of each FSH preparation for 0 to 120 minutes in the presence or absence of 20 μM H89 (PKA inhibitor) (Sigma) or vehicle. At the end of each incubation period (0, 5, 15, 30, 60, 120 minutes), cells were collected and processed for ERK phosphorylation measurement by WB as described previously. Results are expressed as the pERK/total ERK ratio calculated by densitometric analysis of the blots using the Chemidoc MP detection system (BIORAD).

F. β-arr1/2 Silencing by CRISPR/Cas9

After corroborating the identity of the HEK293-hFSHR$^+$ cell line using the AuthentiFiler PCR Amplification Kit (Thermo Fisher Scientific, Waltham, MA, USA), cells were co-transfected with the CRISPR/Cas9 ARRB1 (KN201279G2) and ARRB2 (KN201168G2) (ORIGENE, Rockville, MD) gRNA constructs in the pCas-Guide vector using liposome-mediated endocytosis (TurboFectin, ORIGENE) in OPTIMEM (Life Technologies), following the instructions of the manufacturer. Cells also were cotransfected with donor template DNAs provided by the manufacturer to introduce a cassette containing the green fluorescent protein and puromycin resistance genes to the genome of the target cell by homologous recombination. Control hFSHR$^+$ cells were simultaneously transfected with a negative control CRISPR/Cas9 plasmid (without a specific target) (Scramble, ORIGENE). Forty-eight hours after transfection, cells were treated with 1 μg/mL puromycin (Sigma) and after 3 weeks of treatment, the puromycin-resistant, green fluorescent protein expressing cells were cloned by serial dilution in a 96-well plate. Cloned, puromycin-resistant CRISPR β-arr1/2 HEK293-hFSHR$^+$ KO cells were grown and extracts from confluent cells were then analyzed for β-arrestin 1 and β-arrestin 2 protein expression by WB as described.

G. Measurement of FSH-stimulated Intracellular Ca^{2+} Accumulation by Flow Cytometry

HEK293-hFSHR$^+$ cells grown in 100-mm-diameter cell culture dishes were detached after a brief exposure to trypsin-EDTA (Life Technologies), washed 3 times in PBS, and then transferred to flow cytometry tubes (BD Biosciences, San José, CA) (500×10^3 cells/tube). Cells were then incubated for 30 minutes at 37°C with 3 μM Fura Red (Thermo Fisher Scientific Inc., Waltham, MA), washed 3 times with PBS, resuspended in 500 μL warm (37°C) PBS and fluorescence measured under different conditions [presence (2 mM) or absence of Ca^{2+}, pretreatment with 3 mM EGTA (for 15 minutes before adding FSH, to chelate extracellular Ca^{2+}) or 1 μM thapsigargin (for 20 minutes before FSH exposure, to deplete

intracellular calcium stores and prevent their refilling) in a BD LSRFortessa cytometer (BD Biosciences, Franklin Lakes, NJ) at 480 nm, in the presence or absence of each FSH glycoform at a final concentration of 500 ng/mL. Sample acquisition was performed at low speed. Data extractions were performed using the FlowJo software (BD Biosciences). Data are presented as the relative changes in fluorescence intensity (which reflects intracellular Ca^{2+} [iCa^{2+}] accumulation in response to FSH stimulation) over 300 seconds, taking as 100% the maximal change occurring by exposure to *e*FSH.

H. FSH-stimulated hFSHR Desensitization

For hFSHR desensitization experiments, cultured HEK293-$hFSHR^+$ cells were plated on poly-D-lysine-coated 24-well plates (75×10^3 cells/500 µL) and preincubated for 2 hours in the absence or presence (12 to 100 ng/mL) of each FSH preparation. After the preincubation period, media were removed for secreted (extracellular) cAMP measurement and cells were washed twice with warm PBS, which was replaced with fresh culture medium (with IBMX) containing 1200 ng/mL of each FSH glycoform, and cells returned to the incubator for 30 additional minutes. Thereafter, plates were put on ice and the medium and cells collected for measurement of total cAMP content as described previously.

I. Statistical Analysis

Between-group comparisons to determine statistically significant differences between KDs, as well as ED_{50}, E_{max}, and slope values (kinetic experiments) in the cAMP readouts, and pERK1/2/total ERK ratios at 5 minutes and areas under the curve (AUC), were performed using a least significance difference test after ANOVA followed by the post hoc Duncan's multiple comparison test. Differences in areas under the FSH-stimulated curve in the iCa^{2+} studies were determined using ANOVA or Kruskal-Wallis test followed by either Duncan or Tukey test as appropriate. The Shapiro-Wilk test was used for testing the normal distribution of the data and the Bartlett test for testing homogeneity of variances (particularly when data from multiple replicate experiments were considered). To analyze the simultaneous effects of FSH glycoforms at different concentrations (pERK1/2, desensitization, and dose-response pSOMLuc curves), an analysis of deviance using the doses "en bloc" was used, when only differences between the FSH glycoforms curves were of interest. Experiments were repeated 3 to 8 times in duplicate or triplicate incubations.

3. Results

A. Human FSH Glycoform Extraction and Purification

After extraction of the pituitaries with water, ammonium sulfate precipitation, dialysis, and lyophilization, 16.7 g total protein containing 97.2 mg hFSH immunoactivity was recovered. FSH immunoreactive fractions emerging from a Sephacryl S-100 column were pooled and lyophilized, yielding 91 mg hFSH immunoreactivity in 3.74 g total protein. Four rounds of dual immunoaffinity column chromatography with 15-1.E3.E5 and 4882 mAbs [45, 46] produced purified hFSH as indicated by SDS-PAGE and WB analysis (data not shown). Pooled immunoaffinity chromatography fractions were separated into glycoform fractions by Superdex 75 chromatography (Fig. 2A). Because the 15-1.E3.E5 antibody [45] is a low-affinity antibody, we did not observe any free subunit peak usually generated after elution of hFSH with pH 2.7 buffer. All individual fractions from each hFSH heterodimer peak were analyzed by WB with 15-1.E3.E5 antibody [45] (Fig. 2A, inset). The fractions eluted at the beginning of the heterodimer peak comprised largely the FSH^{24} glycoform, whereas the fractions collected at the end of the peak were mostly the $FSH^{18/21}$ glycoforms [36].

Human FSH glycoform preparations were characterized by SDS-PAGE and FSH subunit Western blots. The Coomassie Blue-stained gels confirmed chemical purity because only the

FSH subunit bands were detected (Fig. 2B). Anti-FSHβ Western blot revealed the presence of ~13% 21 kDA- and ~87% 24kDa-FSHβ in the FSH^{24} preparation (Fig. 2C), whereas the $FSH^{18/21}$ preparation included a significant amount (~73%) of 18kDa-FSHβ. The mobility of the FSH^{24}α band was retarded relative to that of the $FSH^{18/21}$α band, reflecting smaller N-glycans in the latter (Fig. 2D).

4. Functional Studies

A. KD of the FSH Glycoforms Determined by Surface Plasmon Resonance

The KDs resulting from the interaction of each FSH glycoform with the FSHR embedded in liposomes and determined by surface plasmon resonance are shown in Fig. 3A. Although all KDs were in the nanomolar range, the KD value corresponding to *rec*FSH was significantly ($P < 0.01$) higher (6.4 ± 0.8 nM) than those exhibited by the other glycoforms, with the lowest value being 1.4 ± 0.2 nM for *e*FSH, followed by FSH^{24} and $FSH^{18/21}$ (2.9 ± 0.7 and 3.2 ± 0.6 nM, respectively).

B. cAMP Production

Fig. 3B shows total (intra- plus extracellular) cAMP production from HEK293-$hFSHR^+$ cells after 3 hours' incubation in the presence of increasing doses of each FSH glycoform. Both *e*FSH and *rec*FSH evoked the highest total cAMP production levels followed by $FSH^{18/21}$ and FSH^{24} (lower inset in Fig. 3B). The dose necessary to reach E_{max} by *rec*FSH was 100 ng/mL, which was twice the amount required by the other glycoforms. In fact, the highest potency (ED_{50}) for stimulating total cAMP production was exhibited by *e*FSH, followed by $FSH^{18/21}$, FSH^{24}, and *rec*FSH (Fig. 3B, upper inset). The kinetics of FSH glycoform-stimulated maximal cAMP production by HEK293-$hFSHR^+$ cells are shown in Fig. 3C. Maximum cAMP production was reached earlier (40 minutes after FSH exposure) in the presence of *e*FSH, $FSH^{18/21}$, and FSH^{24} than *rec*FSH (which occurred at 60 minutes). The slope of the regression line for the 8 time points analyzed (until maximal cAMP levels were reached), was steeper for *e*FSH (16 ± 1.0) than for the other glycoforms ($FSH^{18/21}$, 12.0 ± 0.6; FSH^{24}, 11.4 ± 0.5; and *rec*FSH, 10.5 ± 0.5) (Fig. 3C inset), confirming the higher potency of the former glycoform over the others.

To compare the cAMP/PKA transcriptional-associated response elicited by the different FSH glycoforms at the hFSHR, HEK293-hFSHR+ (+ supraindex) cells were transfected with the cAMP-sensitive reporter plasmid pSOMLuc. The results showed that all FSH glycoform preparations induced a robust dose-dependent response in luciferase activity, with *e*FSH presenting the highest and FSH^{24} the lowest response (Fig. 3D). In terms of maximal effect, these results were very similar to those observed for total cAMP production.

C. FSH Glycoform-stimulated ERK 1/2 Phosphorylation

We next examined whether different FSH glycoforms exhibited differential effects at the FSHR to trigger ERK1/2 MAPK phosphorylation, a well-known FSHR-mediated effect previously shown to be triggered by both the cAMP/PKA and β-arr1/2 pathways [61, 65–67]. Dose–response curves after 5 minutes' incubation (Fig. 4A) showed unequivocal dose-dependent increases in ERK1/2 phosphorylation resulting from exposure of HEK293-$hFSHR^+$ cells to $FSH^{18/21}$, *e*FSH, and *rec*FSH, whereas the increase in pERK stimulated by FSH^{24} was low at all doses tested (Fig. 4A). In this particular readout for FSH action, $FSH^{18/21}$ evoked the highest response, followed by *e*FSH, although differences between their AUCs did not reach statistical significance; meanwhile, *rec*FSH exhibited an intermediate response and FSH^{24} the lowest one (Fig. 4A). A time-course of ERK1/2 phosphorylation provoked by each FSH glycoform (at a fixed dose of 50 ng/mL) was next performed in HEK293-$hFSHR^+$ cells, and pERK1/2 was analyzed by WB in whole cell

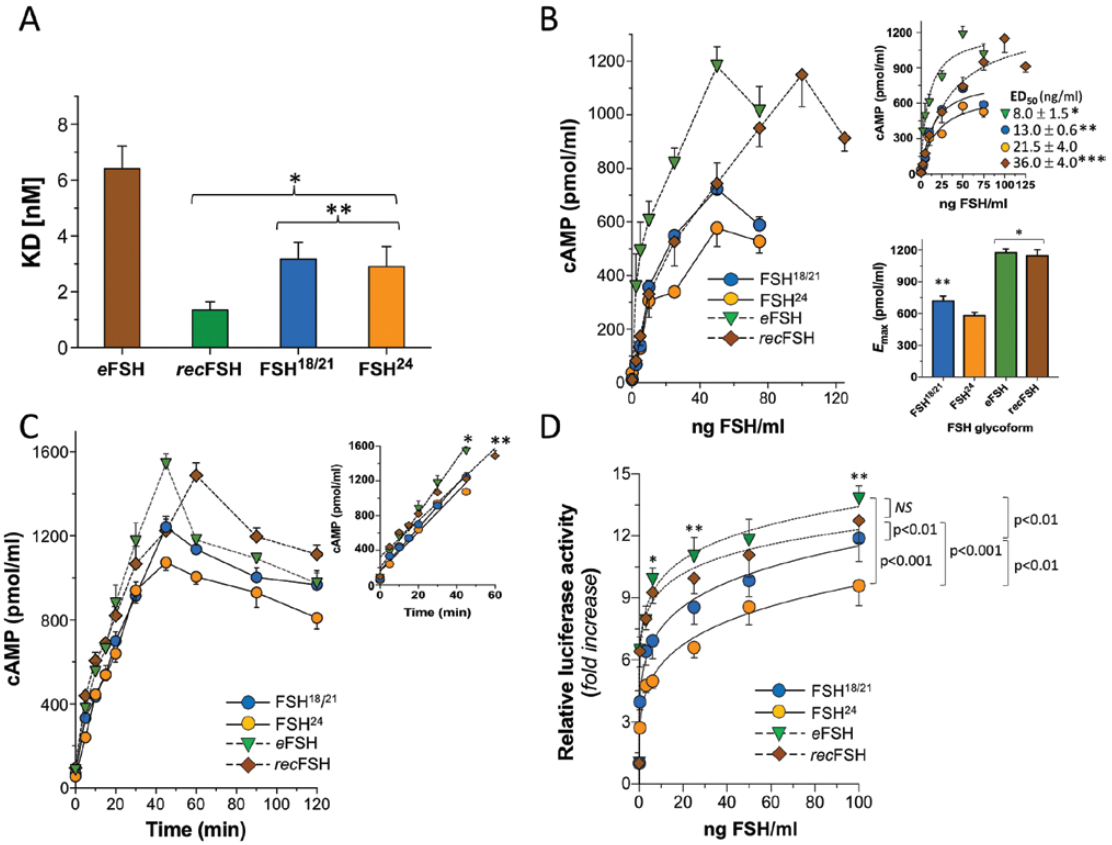

Figure 3. (A) Equilibrium dissociation constant (KD) of FSH glycoforms as assessed by plasmon surface resonance (Biacore). Each bar represents the mean ± SD from 4 independent experiments. *$P < 0.001$ vs *rec*FSH; **$P < 0.01$ vs *e*FSH. (B) Dose-response curves of total (intra- plus extracellular) cAMP production by HEK293-hFSHR^{+} cells exposed to the different FSH glycoforms for 3 hours. Data are presented as mean ± SD from 3 independent experiments. (Upper inset) Nonlinear regression curve of data shown in the main graph with the corresponding ED_{50} values for each glycoform (*$P < 0.01$ *e*FSH vs all others; **$P < 0.05$ $FSH^{18/21}$ vs FSH^{24}; ***$P \leq 0.02$ *rec*FSH vs $FSH^{18/21}$ and FSH^{24}). (Lower inset) E_{max} of each glycoform from the data shown in the main graph (*$P < 0.001$ *e*FSH and *rec*FSH vs $FSH^{18/21}$ and FSH^{24}; **$P = 0.01$ $FSH^{18/21}$ vs FSH^{24}). (C) Kinetic curves of total (intra- plus extracellular) cAMP production by HEK293-hFSHR^{+} cells exposed to 50 ng/mL (*e*FSH, $FSH^{18/21}$, and FSH^{24}) or 100 ng/mL (*rec*FSH) concentrations of FSH glycoforms. (Inset) Linear regression of the curves shown in the main graph, using only points until cAMP production reached maximum values (*$P < 0.01$ *e*FSH vs all other glycoforms; **$P = 0.03$ *rec*FSH vs $FSH^{18/21}$; P = N.S. *rec*FSH vs FSH^{24}, and $FSH^{18/21}$ vs FSH^{24}). (D) Dose-response curves for pSOMLuc expression by HEK293-hFSHR^{+} cells transiently transfected with the cAMP-sensitive pSOMLuc reporter plasmid and exposed to different FSH glycoforms. Each point represents the mean ± SEM of 3 independent experiments. *$P < 0.02$ *e*FSH vs FSH^{24} and *rec*FSH vs FSH24; **eFSH vs FSH24. The levels of significance shown in the right side of the figure correspond to the differences between the FSH glycoform curves considering all doses "en bloc."

lysates. FSH-induced ERK1/2 phosphorylation responses were detected for all FSH glycoforms; the increase in pERK signal was rapid, reaching its maximum after 5 minutes of FSH exposure, then declining progressively during the ensuing 115 minutes. Both early (mainly, but not exclusively dependent on cAMP/PKA) and late (occurring at or after 15 minutes of FSH exposure, and primarily mediated through the β-arr1/2 pathway) pERK responses [61] were significantly higher for $FSH^{18/21}$ (Fig. 4B and Figs. 5A and B). The lowest pERK response was elicited by FSH^{24}, whereas both responses were similar for *e*FSH and *rec*FSH, albeit slightly higher for *e*FSH.

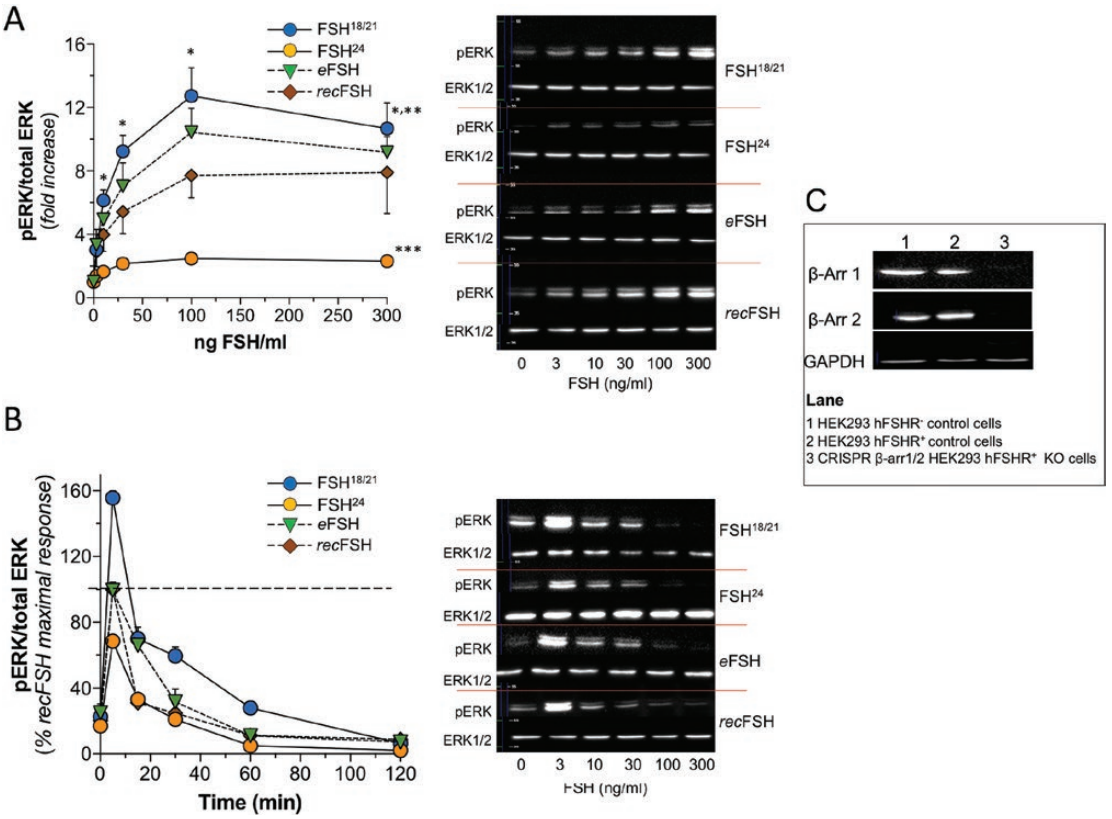

Figure 4. ERK1/2 phosphorylation levels stimulated by exposure of HEK293-hFSHR$^+$ cells to FSH glycoforms. (A) Dose-response curves for ERK phosphorylation stimulated by increasing concentrations of each FSH glycoform. Results are expressed as the pERK/total ERK ratio calculated by densitometric analysis of the blots. Representative immunoblots from a single experiment are shown at the right of the graph. Comparisons among doses and dose-response curves: *$P < 0.03$ FSH$^{18/21}$ vs FSH^{24} at 10, 30, 100, and 300 ng/mL doses; dose-response curves (all doses "en bloc"): **$P < 0.04$ FSH$^{18/21}$ vs *rec*FSH and FSH^{24}; ***$P < 0.01$ FSH^{24} vs *rec*FSH and *e*FSH. (B) ERK1/2 phosphorylation levels during 120 minutes of exposure of HEK293-hFSHR$^+$ cells to 50 ng/mL of each FSH glycoform and quantified by densitometric analysis of the corresponding immunoblots (see Figs. 5A and 5B for statistical comparisons among areas under the pERK1/2 curve and pERK levels at 5 minutes). Representative immunoblots are shown to the right of the graph. Data were normalized to the maximal *rec*FSH-stimulated ERK phosphorylation at 5 minutes, arbitrarily chosen as 100%. Graphs shown in (A) and (B) are the means ± SD of 3 independent experiments. **C.** Representative immunoblot of β-arrestins 1 and 2 in hFSHR$^+$ and hFSHR$^-$control HEK293 cells (lanes 1 and 2, respectively) and in CRISPR β-arr1/2 KO cells (lane 3).

D. FSH Glycoform-stimulated ERK Phosphorylation in CRISPR β-arr1/2 HEK293-hFSHR$^+$ KO Cells

To determine whether FSH glycosylation differentially affects cAMP/PKA- and β-arr1/2-mediated ERK1/2 phosphorylation, CRISPR β-arr1/2 KO and control (not silenced) HEK293-hFSHR$^+$ cells (Fig. 4C) were exposed to 50 ng/mL of each glycoform during 0 to 120 minutes. In all cases, exposure to FSH induced a robust increase in pERK1/2 signal in control cells, whereas in CRISPR β-arr1/2 KO cells a ≲ 40% attenuation at 5 minutes and during the early (0–15 minutes) and, to lesser extent, the late (15–120 minutes) pERK1/2 response was observed (Fig. 6). This decrease in FSH-stimulated ERK1/2 phosphorylation was more evident for FSH$^{18/21}$, in which the pERK response of CRISPR β-arr1/2 KO cells at 5 minutes was 31 ± 9% of that observed in control cells (Figs. 6A and 5C), and significantly ($P \leq 0.01$) lower than those elicited by the other glycoforms in these cells (Fig. 5C and

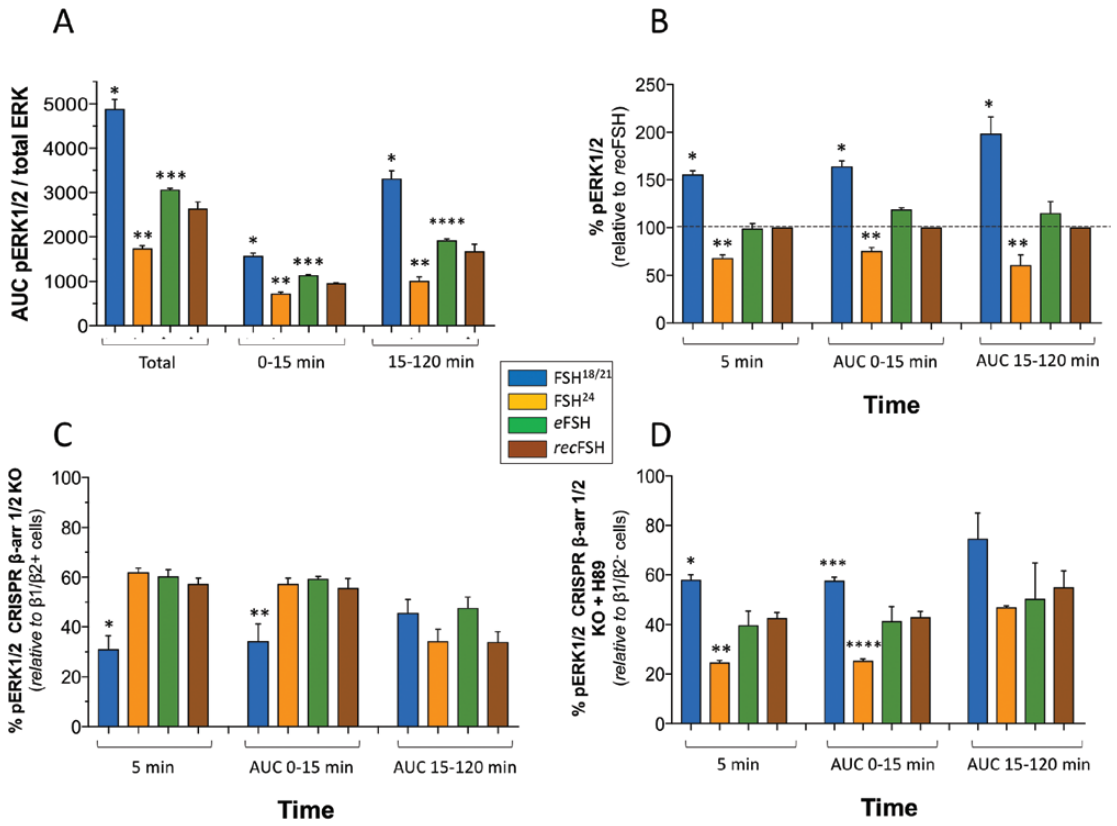

Figure 5. pERK levels at 5 min and areas under the curves (AUC) for the initial (0–15 minutes) and late (15–120) pERK responses to FSH glycoforms. (A) AUC of pERK (total area corresponding to the 0 to 120 minute period as well as to the early (0–15 minutes) and late (15–120 minutes) pERK responses in lysates of HEK293-hFSH^{+} cells exposed to 50 ng/mL of FSH glycoforms (see Fig. 4B). *$P < 0.01$ vs all others; **$P < 0.01$ vs *e*FSH and *rec*FSH; ***$P < 0.01$ vs *rec*FSH; ****$P = 0.05$ vs *rec*FSH. (B) Percent of pERK1/2 normalized to the maximal response of *rec*FSH at 5 minutes, arbitrarily chosen as 100%. *$P < 0.01$ vs all others; **$P < 0.01$ vs *e*FSH. (C) Percent of pERK1/2 in CRISPR β-arr1/2 HEK293-hFSHR^{+} KO cells, relative to control β-arr1/2 non-KO HEK293-hFSHR^{+} cells. *$P < 0.01$ vs all others; **$P \leq 0.05$ vs all others. (D) Percent of pERK1/2 in CRISPR β-arr1/2 HEK293-hFSHR^{+} KO cells in the presence of H89, relative to CRISPR β-arr1/2 HEK293-hFSHR^{+} KO cells in the absence of H89. *$P < 0.01$ vs FSH^{24} and *rec*FSH, and $P < 0.05$ vs *e*FSH; **$P < 0.01$ vs *rec*FSH; ***$P < 0.01$ vs FSH^{24} and *rec*FSH, and $P = 0.05$ vs eFSH; ****$P \leq 0.05$ vs *rec*FSH and *e*FSH.

Figs. 6B-D). Furthermore, the percent decrease in the area under the pERK1/2 curve in CRISPR β-arr1/2 KO cells during the first 0 to 15 minutes of FSH exposure (i.e., the early phase), also was greater for FSH$^{18/21}$ than for FSH^{24}, *rec*FSH, and *e*FSH (Fig. 5C).

To further dissect the contribution of the β-arrestin signaling pathway to FSH glycoform-stimulated ERK1/2 phosphorylation, CRISPR β-arr1/2 HEK293-hFSHR^{+} KO cells were exposed to the PKA inhibitor H89 during FSH stimulation. As shown in digital research materials repository [68] and Fig. 5D, the response of β-arr1/2 KO cells to the FSH glycoforms in the presence of H89 further decreased ERK 1/2 phosphorylation. Nevertheless, the attenuation in FSH-stimulated pERK1/2 response in the presence of H89 was significantly ($P < 0.01$) lower when cells were exposed to FSH$^{18/21}$ than to the other glycoforms (Fig. 5D). Interestingly, concurrent silencing of both β-arrestins (via CRISPR) and PKA signaling (via H89), did not completely suppress pERK phosphorylation to basal levels in response to FSH glycoform stimulation, supporting the view that pathways other than those mediated by PKA and β-arrestin also contribute to FSH-stimulated ERK1/2 phosphorylation, particularly during the 0- to 15-minute initial phase [32, 69].

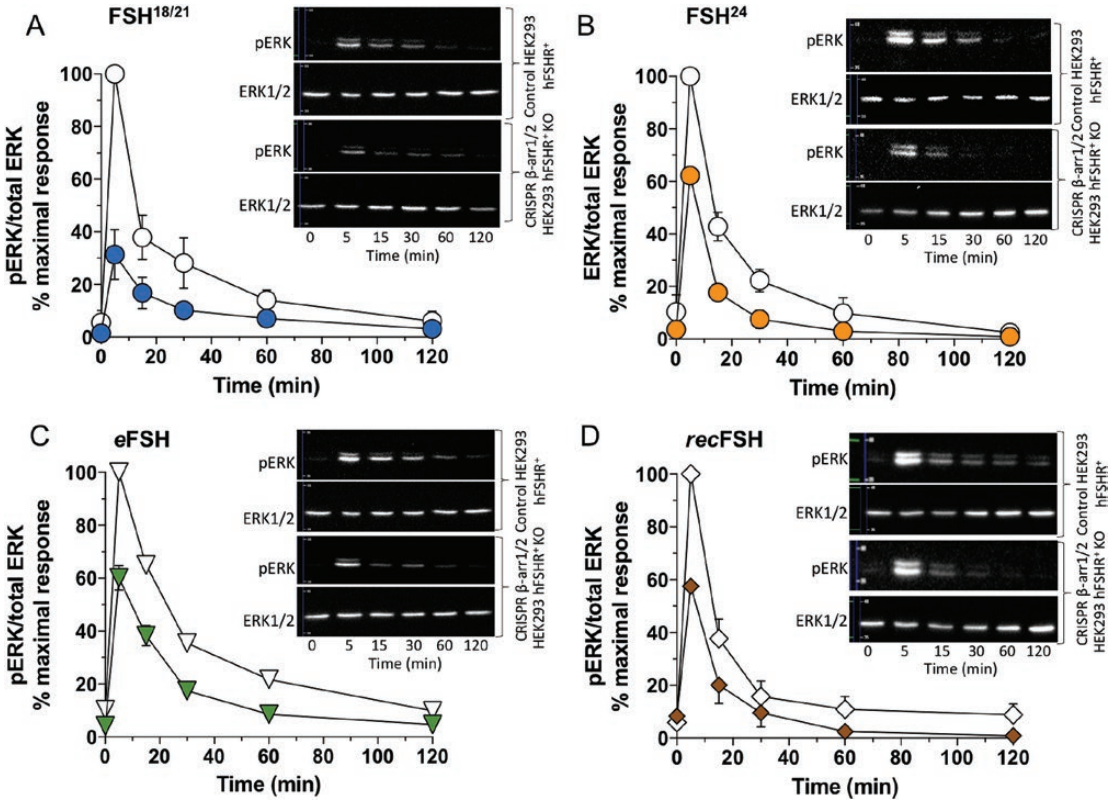

Figure 6. ERK1/2 phosphorylation in control (open symbols) and CRISPR β-arr1/2 HEK293-hFSHR$^+$ KO cells (colored symbols). Each panel (A–D) shows the kinetics of pERK response to 50 ng of each glycoform. Results are expressed as the pERK/total ERK ratio calculated by densitometric analysis of the blots; data were normalized to the maximal ERK phosphorylation response in control cells at 5 minutes, arbitrarily chosen as 100%. The insets show representative immunoblots for each glycoform in control and KO HEK293 cells. Because the pERK signal for FSH^{24} was weak (see Fig. 4A), the blot shown in the inset was overexposed to better appreciate the differences between control and β-arr1/2 KO HEK293-hFSHR$^+$ cells. See Fig. 5C for statistical differences between the glycoforms.

E. FSH-stimulated Intracellular Ca^{2+} Accumulation

To determine whether FSH glycoforms provoke Ca^{2+} mobilization through similar or distinct mechanisms (T-type Ca^{2+} channels and/or Ca^{2+} mobilization from intracellular stores [70–78]), HEK293-hFSHR$^+$ cells were exposed to 500 ng/mL of each FSH glycoform under different conditions (presence/absence of extracellular calcium or depletion of iCa^{2+} stores) for 240 seconds, and iCa^{2+} accumulation was detected by flow cytometry. As shown in the digital research materials repository [68], exposure of HEK293-hFSHR$^+$ cells to high-dose FSH led to a rapid decrease in Fura Red dye fluorescence (expressed as changes in mean fluorescence intensity), starting at ~70 to 80 seconds and returning to baseline levels at ~ 160 to 180 seconds after addition of FSH. Nevertheless, the effect of each FSH glycoform on Ca^{2+} mobilization varied depending on the particular experimental condition. In the presence of extracellular Ca^{2+} in the PBS incubation buffer, exposure to *e*FSH provoked the highest effect on iCa^{2+} accumulation, followed by *rec*FSH, and FSH^{24} and FSH$^{18/21}$, with the effect of the latter 2 overlapping (Fig. 7A and digital research materials repository [68]). Omission of Ca^{2+} from PBS, decreased the iCa^{2+} response by 25 ± 6% (*e*FSH), 29 ± 6% (*rec*FSH), 10 ± 3% (FSH$^{18/21}$), and 33 ± 7% (FSH^{24}) (Figs. 7B and digital research materials repository [68]), with the addition of EGTA in the incubation buffer yielding similar results (Figs. 7C and S2C). Meanwhile, pretreatment with thapsigargin further decreased iCa^{2+} accumulation stimulated by all glycoforms (>50% decrease in iCa^{2+} response): Figs. 7D and

digital research materials repository [68]. As shown, the iCa^{2+} response to $FSH^{18/21}$ was the most profoundly affected by thapsigargin pretreatment (Fig. 7D and digital research materials repository [68]), with levels ~80% below those observed in the absence of this Ca^{2+} ATPase inhibitor and the presence of extracellular Ca^{2+}. These data indicate that all FSH glycoforms stimulate Ca^{2+} mobilization in HEK293-$hFSHR^{+}$ cells through both T-type Ca^{2+} channels and intracellular stores, but predominantly through the latter when stimulated by $FSH^{18/21}$.

F. FSH-stimulated hFSHR Desensitization

Desensitization of the FSHR to FSH glycoform stimulation in HEK293-hFSHR + cells was next examined (Fig. 8). Initially, cells were incubated with increasing doses (0-100 ng/mL) of FSH glycoforms for 2 hours and then reexposed to a high (1200 ng/mL) concentration of the corresponding glycoform for 30 additional minutes. During the first 2 hours of incubation, all glycoforms elicited a robust increase in extracellular cAMP accumulation (Fig. 8A). Upon reexposure to the high agonist dose, the FSHR displayed desensitization regardless of the FSH glycoform and dose used during pretreatment (Fig. 8B). Nevertheless, receptor desensitization to the high FSH glycoform dose was significantly ($P < 0.01$) attenuated for *e*FSH at all preexposure doses and for *rec*FSH at the 10 to 50 ng/mL doses, compared with reexposure to $FSH^{18/21}$ and FSH^{24}, which exhibited a more profound level of FSHR desensitization. In the latter glycoforms, desensitization provoked by exposure to the high FSH glycoform dose for 30 minutes was very similar, except in cells prestimulated with the highest dose (100 ng/mL) of $FSH^{18/21}$, in which the cAMP response upon FSH re-exposure was significantly ($P < 0.01$) lower.

5. DISCUSSION

Despite the fact that FSH binding has been considered to exclusively be a protein-protein interaction, variations in glycosylation (either as micro- or macroheterogeneity) has been known for a long time to influence the response of the target cell to the FSH stimulus [8, 11, 28, 62, 79, 80]. To analyze the impact of oligosaccharide heterogeneity on hFSH activity, we here studied the in vitro bioactivities of the 2 major, naturally occurring pituitary hFSH glycoforms $FSH^{18/21}$ and FSH^{24} at the hFSHR stably expressed in HEK293 cells and compared these activities with those exhibited by 2 other FSH preparations exhibiting distinct glycosylation patterns. Although earlier studies have shown that FSHR density in target cells plays a role in determining the preference of signaling cascades used [52, 81], this was not of concern as apparently the density of FSHR in our stably transfected HEK293-$hFSHR^{+}$ cells was kept constant. The finding that the FSH^{24} preparation contained a small amount of FSH^{21} in FSH^{24} was not a major concern because we have observed that when 1 glycoform contains ≥ 80% of the preparation, it behaves as if it is 100% (unpublished observations).

Keeping in mind the possibility that these FSH glycoforms might exhibit some degree of functional selectivity or biased agonism at the hFSHR [67], the in vitro bioassays used addressed different biochemical readouts stimulated through distinct downstream pathways. The results showed that the ability of hFSH glycoforms to stimulate each of these endpoints varied depending on the particular glycoform tested. In the cAMP accumulation, cAMP/PKA-mediated transcriptional response, and ERK1/2 phosphorylation bioassays, hypo-glycosylated $FSH^{18/21}$ always was more potent/active than the fully glycosylated FSH^{24} glycoform, whereas *e*FSH showed the greatest potency/activity in the cAMP and pSOM-Luc assays but not in the pERK1/2 dose-response assay, in which $FSH^{18/21}$ was the most active glycoform. In all of these assays, and particularly in the pERK1/2 assay, FSH^{24} was the least potent/active glycoform among all preparations tested. These observations suggested biased agonism of *e*FSH for the Gs-cAMP-PKA-CREB pathway and of $FSH^{18/21}$ for the ERK1/2 activation path. The differences in potency between $FSH^{18/21}$ and FSH^{24}

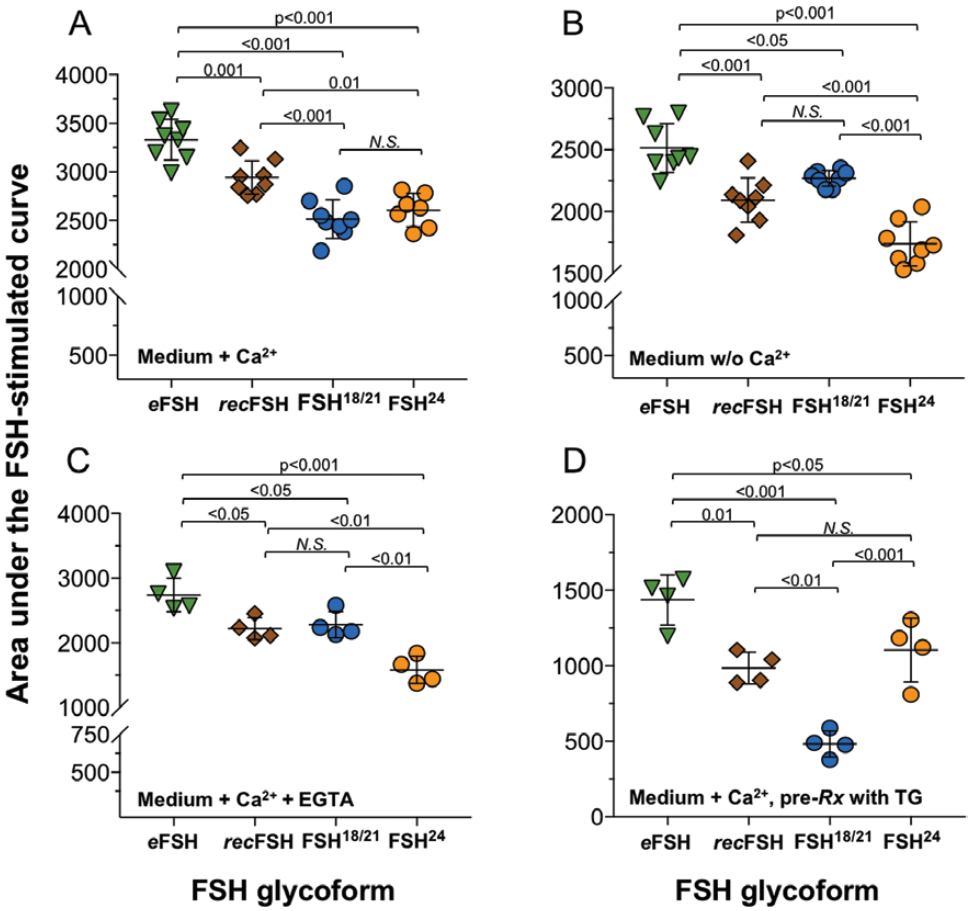

Figure 7. Intracellular iCa^{2+}accumulation in HEK293-hFSHR + cells expressed as the area under the FSH-stimulated curve calculated from the data presented in the digital research materails repository [68]. Areas under the curve were calculated considering the first significant change in fluorescence (1/n mean fluorescence intensity) following addition of FSH and the last value of the fluorescence descending curve before reaching baseline levels (see curves in the digital research materails repository [68]). Each panel corresponds to different conditions (A and B) presence or absence of Ca^{2+} in the incubation buffer, (C) addition of EGTA, (D) or pretreatment with thapsigargine (TG) before FSH addition. Each symbol represents the normalized result of an independent experiment (see Fig. S2); horizontal and vertical lines indicate the mean ± SD from 4 to 8 independent experiments, respectively. Differences among FSH glycoform responses are shown on the top of each graph. N.S.: not significant. Different scales in the Y-axes were used to allow better appreciation of the differences among glycoforms.

on the Gs-cAMP-PKA signaling pathway observed in the present study follow the pattern previously reported for recombinant GH_3-expressed hFSH glycoform preparations in stimulating KGN cells [26]. Although both pituitary hFSH and recombinant GH_3-derived hFSH show many similarities in oligosaccharide structure (i.e., in microheterogeneity), there are some differences that mainly include variations in the relative abundance/frequency of triantennary and biantennary glycans as well as in glycan size and flexibility [36], which apparently are not relevant for binding at the FSHR as both pituitary and GH_3-derived hypo- and tetra-glycosylated FSH glycoforms displayed similar differences in FSHR binding when tested in heterologous and homologous radioreceptor binding assays, with $FSH^{18/21}$ showing higher binding activity than FSH^{24} [25, 36], albeit they share similar Kds at the hFSHR, as was observed in the present study [36]. Further, it has been reported that for both pituitary and recombinant GH_3-derived $FSH^{18/21}$ glycoforms, more FSH binding sites are available than for their corresponding FSH^{24} counterparts [25, 36], which may be one of the

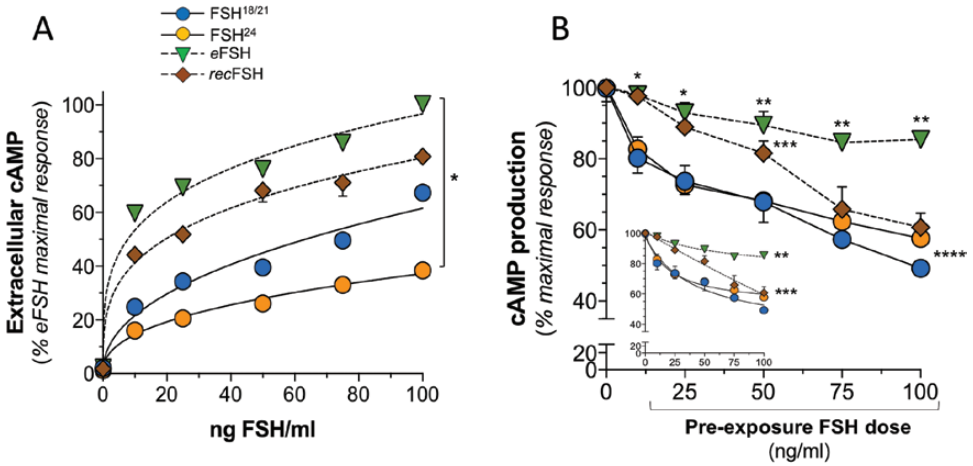

Figure 8. Desensitization of the hFSHR in HEK293-hFSHR^{+} cells exposed to different FSH glycoforms. (A) Cells were stimulated for 2 hours with increasing amounts of each glycoform in the presence of IBMX, and cAMP in the incubation media was measured by RIA. *All treatments were significantly different from each other at $P < 0.01$. (B) After stimulation with FSH, cells were washed twice and then rechallenged with a saturating (1200 ng/mL) dose of each FSH glycoform in the presence of IBMX; total (intra- and extracellular) cAMP was then determined. *$P < 0.01$ *e*FSH and *rec*FSH *vs* FSH$^{18/21}$ and FSH^{24} in cells preexposed to 10 and 25 ng/mL FSH; **$P < 0.01$ *e*FSH vs all other glycoforms in cells preexposed to 50, 75, and 100 ng/mL FSH; ***$P < 0.01$ *rec*FSH vs FSH$^{18/21}$ and FSH^{24} in cells preexposed to 50 ng/mL; ****$P < 0.01$ FSH$^{18/21}$ vs FSH^{24} and *rec*FSH at the 100 ng/mL preexposed FSH dose. Inset: Nonlinear regression of the data shown in the main graph. Level of significant differences among the glycoform curves in the inset graph (all doses "en bloc"): **$P < 0.01$ *e*FSH vs all other glycoforms; ***$P < 0.01$ *rec*FSH vs FSH$^{18/21}$ and FSH^{24}.

mechanisms through which activation of the Gs-cAMP-PKA pathway is higher for FSH$^{18/21}$. The high potency of *e*FSH in the cAMP accumulation and cAMP-PKA transcriptional activation assays is not surprising given that this particular preparation has been shown to be highly active when its binding is compared with its counterparts in other species, including humans [4, 82, 83]. In this vein, besides being predominantly hypo-glycosylated (Fig. 1), oligosaccharides in *e*FSHα-subunit (at Asn^{56}) are predominantly biantennary and smaller than in pituitary hFSH and the structure of the determinant loop of its β-subunit differs from those of other FSH preparations [4, 34], which may facilitate binding to and activation of the FSHR. In the case of *rec*FSH the most outstanding differences lie in that its oligosaccharides are predominantly biantennary and lack sialic acid linked α2-6, which may also facilitate receptor activation and Gs-cAMP-PKA signaling, by as-yet-unknown mechanisms. Finally, an additional mechanism through which *e*FSH and *rec*FSH may have exhibited higher efficacy than hypo- and fully glycosylated hFSH could be the attenuated desensitization of the hFSHR when stimulated by the former compounds versus the latter as shown in the present study.

Like many GPCRs belonging to family A of the GPCR superfamily, the FSHR stimulates ERK1/2 phosphorylation through several mechanisms, mainly activation of the Gs/cAMP/PKA and the β-arr1/2 pathways, but also using the G_i and $G_{q/11}$ signaling cascades [32, 61, 84]. Given this array of pathways, it is thus feasible that upon binding to the FSHR different FSH ligands may provoke distinct conformational rearrangements within the transmembrane domains of the receptor leading to stabilization of a conformation that may facilitate preferential activation of one particular pathway or a subset of pathways leading to differentially mediated signaling (e.g., on ERK1/2 signaling) resulting in an imbalanced or biased response. In the FSHR, the kinetics of Gs/cAMP/PKA- and β-arr1/2-mediated ERK1/2 activation in heterologous cell systems follows a pattern where β-arr1/2-mediated pERK1/2 is delayed and more sustained compared with the Gs/cAMP/PKA-dependent pathway, which is transient but occurs earlier [61]. Nevertheless, it has been shown that in HEK293 cells

expressing the hFSHR, transient silencing of β-arr1/2 by siRNA also may have a variable effect on the early ERK1/2 phosphorylation response to agonist [61, 62, 85]. Further, it was more recently shown that depletion of β-arrestins in 3 different parental HEK293 cell lines by either siRNA or CRISPR/Cas9, equally affected the early phase of ERK1/2 activation in response to FSH exposure [69].

We used HEK293-hFSHR^{+} cells in which β-arr1/2 were knocked out by CRISPR/Cas9 to determine whether macroheterogeneity in the pituitary FSH molecule may promote differential/biased signaling at the hFSHR to stimulate ERK1/2 phosphorylation. These experiments revealed that the ERK1/2 activation response of CRISPR β-arr1/2 hFSHR^{+} KO cells to FSH$^{18/21}$ was more profoundly affected than when cells were exposed to the other glycoforms, which responded in a similar manner (Fig. 5C). These data strongly suggest that the ERK1/2 response to hypo-glycosylated hFSH is, comparatively, more arrestin-dependent (but not G protein-independent) than the other glycoforms. Further, exposure of CRISPR β-arr1/2 KO cells to the PKA inhibitor H89 had less impact on FSH$^{18/21}$-stimulated ERK1/2 phosphorylation than on the response to the other glycoforms. This result was unexpected given the robust cAMP response of the HEK293-hFSHR^{+} cells to FSH exposure, particularly to *e*FSH and *rec*FSH. The complete lack of suppression of ERK1/2 activation in the presence of both PKA inhibitor and β-arr1/2 silencing, indicates that alternative pathways may be operating in our experimental model to activate FSH-stimulated ERK1/2 signaling. In this vein, it has been shown that activation of the pertussis-sensitive $G_{i/o}$ protein plays an important role on biased ERK1/2 activation in other GPCRs [86] as well as on cell proliferation mediated by the FSHR in maturing mouse Sertoli cells [84]. Signal rewiring in CRISPR/Cas9 genome-edited cells to pathways other than the Gs- and β-arr1/2-mediated pathways also might be contributing to the incomplete suppression of ERK1/2 activation in the presence of PKA inhibition and β-arrestin silencing [69].

The complexity of signaling mediated by the activated FSHR includes Ca^{2+}-mediated signaling pathways. In this regard, it has been established that high-dose FSH stimulation induces an increase in iCa^{2+} levels in both rat granulosa cells and Sertoli cells [70, 73, 74, 76, 77]. This increase in FSH-stimulated iCa^{2+} accumulation may be attributed to different mechanisms including influx of extracellular Ca^{2+} through T-type Ca^{2+} channels and release from intracellular stores [70, 71, 76, 78, 87, 88]. Further, it has been shown that in HEK293 and KGN cells transiently expressing the hFSHR, cytosolic Ca^{2+} increase may also occur through interaction between APPL-1 and the first intracellular loop of the hFSHR, involving inositol 1,4,5-trisphosphate (IP_3) accumulation presumably *via* $G\alpha_q$-PLCβ activation [70]. In the present study, we analyzed the effects of different FSH glycoforms on cytosolic Ca^{2+} accumulation under different conditions that may facilitate identification of the mechanisms whereby the glycoforms could preferentially stimulate cytosolic Ca^{2+} accumulation. The results showed that all 4 FSH glycoforms evoked iCa^{2+} accumulation through both of the previously mentioned mechanisms. Remarkably, FSH$^{18/21}$ was the least potent glycoform to stimulate Ca^{2+} mobilization from intracellular stores when the cells were depleted of intracellular Ca^{2+} by preventing their refilling through preexposure to thapsigargin, indicating that this source of Ca^{2+} plays a major role in FSH$^{18/21}$-stimulated cytosolic Ca^{2+} accumulation. The mechanism(s) subserving this selectivity of FSH$^{18/21}$ towards iCa^{2+} stores might involve IP_3 accumulation via $G\alpha_q$ activation of PLCβ or other PLC isoenzymes associated with other intracellular regulators [89]. In this vein, it has been previously shown that the closely-related LH/chorionic gonadotropin receptor and TSH receptor also activate $G_{q/11}$, stimulate phospholipase C, and increase second messengers such as inositol phosphates, calcium, and diacylglycerol [89–95]. Whatever mechanisms are involved in FSH-stimulated mobilization of Ca^{2+} from intracellular stores, the results of the present study indicate that FSH$^{18/21}$ preferentially stimulates the release of Ca^{2+} from this source over that mediated by Ca^{2+} plasma membrane channels, as is the case of the other glycoforms.

Assessment of FSH glycoform-provoked hFSHR desensitization, revealed an interesting pattern, with cells reexposed to *e*FSH and *rec*FSH exhibiting a significantly attenuated refractoriness to further agonist stimulation than those reexposed to FSH$^{18/21}$ and FSH^{24}.

These differences might be due to particular configurations adopted by the hFSHR when activated by the human pituitary glycoforms (see the following section), which might facilitate receptor phosphorylation by receptor kinases (GRK2 and 3) and hence $G\alpha_s$ uncoupling [61, 66, 96], while prolonging this G protein response to *e*FSH and *rec*FSH.

The molecular mechanisms subserving the differential effects of hypo- and tetra-glycosylated FSH isoforms remain largely unknown, particularly considering that in the most recent crystal structure of the entire hFSHR extracellular domain in complex with FSH revealed that FSH glycans do not participate in binding to the receptor because they appear oriented away from the hormone-receptor interface, rather being sequestered at the periphery of complex [97]. Nevertheless, given the essential role of FSH carbohydrates for full receptor activation and signaling, it is highly possible that they may affect both stability and conformational flexibility of the FSH dimer and thereby affect the association kinetics with the FSHR [29] and secondarily on receptor activation, with hypo-glycosylated pituitary FSH engaging the receptor faster than its tetra-glycosylated counterpart [25]. In addition, hypo-glycosylated FSH also occupies more FSHRs than tetra-glycosylated FSH and exhibits higher in vitro binding activity in some systems [25, 36]. Given that hypo-glycosylated FSH also exhibited a preference for particular signaling pathways (e.g., β-arrestin/ERK1/2 and/or Gi/ERK1/2 vs Gs-cAMP-PKA/ERK1/2 pathways, and Gq/11 vs T-type Ca^{2+} channels to provoke cytosolic Ca^{2+} accumulation), it is also possible that oligosaccharides may additionally influence the final receptor conformation and association with other FSHR molecules and/or partners [20, 21, 97] via distinct association/dissociation kinetics with the receptor that could in turn eventually define the signaling pathways to be selectively or preferentially activated/inhibited from the wide repertoire of associated effectors. In fact, preferential activation of distinct signaling pathways by charge variants of FSH and partially deglycosylated equine LH has been recognized [10, 11, 30, 62, 79, 98] and, more recently, another study showed that the oligosaccharide complexity of recombinant hFSH preparations differentially affected gene expression and steroidogenesis in cultured human granulosa cells [80]. Thus, not only macroheterogeneity but also microheterogeneity in FSH preparations appear to influence the biological responses to gonadotropin stimulation at the target cell level.

It has been widely demonstrated that the relative abundance of FSH glycoforms varies depending on the phase of the menstrual cycle. In serum from normal menstruating women, the abundance of less acidic/more basic isoforms and concentrations of hypo-glycosylated FSH glycoforms is higher during the midcycle than in other cycle phases [99–103], and the content of $FSH^{18/21}$ in the pituitaries of women decreases almost linearly with age throughout reproductive life [5, 43]. Differences in the relative abundance of FSH glycoforms during the menstrual cycle as well as in their distinct effects at the target cell, which are determined by differential glycosylation, offer a potential therapeutic avenue for the design of novel strategies based on the administration of recombinant FSH glycoforms in varying ratios and combinations that may mimic what occurs physiologically during the normal menstrual cycle, and thereby improve the outcomes and minimize side effects of controlled ovarian hyperstimulation with gonadotropins in infertile women.

Acknowledgments

Financial Support: This study was supported by grants 240619 from CONACyT (Consejo Nacional de Ciencia y Tecnología), México and the National University of Mexico (UNAM) (to A. Ulloa-Aguirre), and from grant AG029531 from the National Institutes of Health (NIH), Bethesda, Maryland (to G.R. Bousfield).

Additional Information

Correspondence and Reprint Requests: Alfredo Ulloa-Aguirre, MD, DSc, Scientific Director, RAI, UNAM, Instituto Nacional de Ciencias Médicas y Nutrición SZ, Vasco de Quiroga 15, Tlalpan, CP 14000, Mexico City, Mexico. E-mail: aulloaa@unam.mx.

Disclosure Summary: The authors have nothing to disclose

Data availability: The datasets generated during/or analyzed during the current study are not publicly available but are available from the corresponding author on reasonable request.

References

1. Baenziger JU. Glycoprotein hormone GalNAc-4-sulphotransferase. *Biochem Soc Trans*. 2003;**31**(2):326–330.
2. Chappel SC, Ulloa-Aguirre A, Coutifaris C. Biosynthesis and secretion of follicle-stimulating hormone. *Endocr Rev*. 1983;**4**(2):179–211.
3. Pierce JG, Parsons TF. Glycoprotein hormones: structure and function. *Annu Rev Biochem*. 1981;**50**:465–495.
4. Bousfield GR, Butnev VY, Gotschall RR, Baker VL, Moore WT. Structural features of mammalian gonadotropins. *Mol Cell Endocrinol*. 1996;**125**(1-2):3–19.
5. Bousfield GR, Butnev VY, Rueda-Santos MA, Brown A, Hall AS, Harvey DJ. Macro- and microheterogeneity in pituitary and urinary follicle-stimulating hormone glycosylation. *J Glycomics Lipidomics*. 2014;**4**:125–141.
6. Bousfield GR, Butnev VY, Walton WJ, et al. All-or-none N-glycosylation in primate follicle-stimulating hormone beta-subunits. *Mol Cell Endocrinol*. 2007;**260-262**:40–48.
7. Davis JS, Kumar TR, May JV, Bousfield GR. Naturally occurring follicle-stimulating hormone glycosylation variants. *J Glycomics Lipidomics*. 2014;**4**(1):e117.
8. Walton WJ, Nguyen VT, Butnev VY, Singh V, Moore WT, Bousfield GR. Characterization of human FSH isoforms reveals a nonglycosylated beta-subunit in addition to the conventional glycosylated beta-subunit. *J Clin Endocrinol Metab*. 2001;**86**(8):3675–3685.
9. Creus S, Chaia Z, Pellizzari EH, Cigorraga SB, Ulloa-Aguirre A, Campo S. Human FSH isoforms: carbohydrate complexity as determinant of in-vitro bioactivity. *Mol Cell Endocrinol*. 2001;**174**(1-2):41–49.
10. Timossi CM, Barrios de Tomasi J, Zambrano E, González R, Ulloa-Aguirre A. A naturally occurring basically charged human follicle-stimulating hormone (FSH) variant inhibits FSH-induced androgen aromatization and tissue-type plasminogen activator enzyme activity in vitro. *Neuroendocrinology*. 1998;**67**(3):153–163.
11. Timossi CM, Barrios-de-Tomasi J, González-Suárez R, et al. Differential effects of the charge variants of human follicle-stimulating hormone. *J Endocrinol*. 2000;**165**(2):193–205.
12. Ulloa-Aguirre A, Midgley AR Jr, Beitins IZ, Padmanabhan V. Follicle-stimulating isohormones: characterization and physiological relevance. *Endocr Rev*. 1995;**16**(6):765–787.
13. Ulloa-Aguirre A, Timossi C, Barrios-de-Tomasi J, Maldonado A, Nayudu P. Impact of carbohydrate heterogeneity in function of follicle-stimulating hormone: studies derived from in vitro and in vivo models. *Biol Reprod*. 2003;**69**(2):379–389.
14. Ulloa-Aguirre A, Timossi C, Damián-Matsumura P, Dias JA. Role of glycosylation in function of follicle-stimulating hormone. *Endocrine*. 1999;**11**(3):205–215.
15. Bishop LA, Nguyen TV, Schofield PR. Both of the beta-subunit carbohydrate residues of follicle-stimulating hormone determine the metabolic clearance rate and in vivo potency. *Endocrinology*. 1995;**136**(6):2635–2640.
16. Matzuk MM, Boime I. The role of the asparagine-linked oligosaccharides of the alpha subunit in the secretion and assembly of human chorionic gonadotrophin. *J Cell Biol*. 1988;**106**(4):1049–1059.
17. Sairam MR. Role of carbohydrates in glycoprotein hormone signal transduction. *Faseb J*. 1989;**3**(8):1915–1926.
18. Sairam MR, Bhargavi GN. A role for glycosylation of the alpha subunit in transduction of biological signal in glycoprotein hormones. *Science*. 1985;**229**(4708):65–67.
19. Valove FM, Finch C, Anasti JN, Froehlich J, Flack MR. Receptor binding and signal transduction are dissociable functions requiring different sites on follicle-stimulating hormone. *Endocrinology*. 1994;**135**(6):2657–2661.
20. Jiang X, Dias JA, He X. Structural biology of glycoprotein hormones and their receptors: insights to signaling. *Mol Cell Endocrinol*. 2014;**382**(1):424–451.
21. Jiang X, Fischer D, Chen X, et al. Evidence for follicle-stimulating hormone receptor as a functional trimer. *J Biol Chem*. 2014;**289**(20):14273–14282.
22. Fox KM, Dias JA, Van Roey P. Three-dimensional structure of human follicle-stimulating hormone. *Mol Endocrinol*. 2001;**15**(3):378–389.

23. Bishop LA, Robertson DM, Cahir N, Schofield PR. Specific roles for the asparagine-linked carbohydrate residues of recombinant human follicle stimulating hormone in receptor binding and signal transduction. *Mol Endocrinol.* 1994;**8**(6):722–731.
24. Flack MR, Froehlich J, Bennet AP, Anasti J, Nisula BC. Site-directed mutagenesis defines the individual roles of the glycosylation sites on follicle-stimulating hormone. *J Biol Chem.* 1994;**269**(19):14015–14020.
25. Bousfield GR, Butnev VY, Butnev VY, Hiromasa Y, Harvey DJ, May JV. Hypo-glycosylated human follicle-stimulating hormone (hFSH(21/18)) is much more active in vitro than fully-glycosylated hFSH (hFSH(24)). *Mol Cell Endocrinol.* 2014;**382**(2):989–997.
26. Jiang C, Hou X, Wang C, et al. Hypoglycosylated hFSH has greater bioactivity than fully glycosylated recombinant hFSH in human granulosa cells. *J Clin Endocrinol Metab.* 2015;**100**(6): E852–E860.
27. Wang H, Butnev V, Bousfield GR, Kumar TR. A human FSHB transgene encoding the double N-glycosylation mutant (Asn(7Δ) Asn(24Δ)) FSHβ subunit fails to rescue Fshb null mice. *Mol Cell Endocrinol.* 2016;**426**:113–124.
28. Wang H, May J, Butnev V, et al. Evaluation of in vivo bioactivities of recombinant hypo- (FSH21/18) and fully- (FSH24) glycosylated human FSH glycoforms in Fshb null mice. *Mol Cell Endocrinol.* 2016;**437**:224–236.
29. Meher BR, Dixit A, Bousfield GR, Lushington GH. Glycosylation effects on FSH-FSHR interaction dynamics: a case study of different FSH Glycoforms by Molecular Dynamics Simulations. *Plos One.* 2015;**10**(9):e0137897.
30. Barrios-De-Tomasi J, Timossi C, Merchant H, Quintanar A, Avalos JM, Andersen CY, Ulloa-Aguirre A. Assessment of the in vitro and in vivo biological activities of the human follicle-stimulating isohormones. *Mol Cell Endocrinol.* 2002;**186**:189–198.
31. Ulloa-Aguirre A, Reiter E, Crépieux P. FSH receptor signaling: complexity of interactions and signal diversity. *Endocrinology.* 2018;**159**(8):3020–3035.
32. Casarini L, Crepieux P. Molecular mechanisms of action of FSH. *Front Endocrinol (Lausanne).* 2019;**10**:305.
33. Michel MC, Charlton SJ. Biased agonism in drug discovery-is it too soon to choose a path? *Mol Pharmacol.* 2018;**93**(4):259–265.
34. Dalpathado DS, Irungu J, Go EP, Butnev VY, Norton K, Bousfield GR, Desaire H. Comparative glycomics of the glycoprotein follicle stimulating hormone: glycopeptide analysis of isolates from two mammalian species. *Biochemistry.* 2006;**45**:8665–8673.
35. Riccetti L, Sperduti S, Lazzaretti C, et al. Glycosylation pattern and in vitro bioactivity of reference follitropin alfa and biosimilars. *Front Endocrinol (Lausanne).* 2019;**10**:503.
36. Butnev VY, Butnev VY, May JV, et al. Production, purification, and characterization of recombinant hFSH glycoforms for functional studies. *Mol Cell Endocrinol.* 2015;**405**:42–51.
37. Bousfield GR, Butnev VY, White WK, Hall AS, Harvey DJ. Comparison of follicle-stimulating hormone glycosylation microheterogenity by quantitative negative mode nano-electrospray mass spectrometry of peptide-N glycanase-released oligosaccharides. *J Glycomics Lipidomics.* 2015;**5**:129–146.
38. Gervais A, Hammel YA, Pelloux S, et al. Glycosylation of human recombinant gonadotrophins: characterization and batch-to-batch consistency. *Glycobiology.* 2003;**13**(3):179–189.
39. Hård K, Mekking A, Damm JB, et al. Isolation and structure determination of the intact sialylated N-linked carbohydrate chains of recombinant human follitropin expressed in Chinese hamster ovary cells. *Eur J Biochem.* 1990;**193**(1):263–271.
40. Renwick AG, Mizuochi T, Kochibe N, Kobata A. The asparagine-linked sugar chains of human follicle-stimulating hormone. *J Biochem.* 1987;**101**:1209–1221.
41. Baenziger JU, Green ED. Pituitary glycoprotein hormone oligosaccharides: structure, synthesis and function of the asparagine-linked oligosaccharides on lutropin, follitropin and thyrotropin. *Biochim Biophys Acta.* 1988;**947**(2):287–306.
42. Green ED, Baenziger JU. Asparagine-linked oligosaccharides on lutropin, follitropin, and thyrotropin. II. Distributions of sulfated and sialylated oligosaccharides on bovine, ovine, and human pituitary glycoprotein hormones. *J Biol Chem.* 1988;**263**:36–44.
43. Bousfield GR, Harvey DJ. Follicle-stimulating hormone glycobiology. *Endocrinology.* 2019;**160**(6):1515–1535.
44. Fevold HL, Hisaw FL, Leonard SL. The gonad stimulating and the luteinizing hormones of the anterior lobes of the hypophysis. *Am J Physiol.* 1931;**97**:291–301.
45. RRID AB_2814844,https//scicrunch.org/resolver/AB_2814844.

46. RRID AB_2814867, https//scicrunch.org/resolver/AB_2814867.
47. Bousfield GR, Ward DN. Purification of lutropin and follitropin in high yield from horse pituitary glands. *J Biol Chem*. 1984;**259**(3):1911–1921.
48. Tilly JL, Aihara T, Nishimori K, et al. Expression of recombinant human follicle-stimulating hormone receptor: species-specific ligand binding, signal transduction, and identification of multiple ovarian messenger ribonucleic acid transcripts. *Endocrinology*. 1992;**131**(2):799–806.
49. O'Shannessy DJ, Brigham-Burke M, Soneson KK, Hensley P, Brooks I. Determination of rate and equilibrium binding constants for macromolecular interactions using surface plasmon resonance: use of nonlinear least squares analysis methods. *Anal Biochem*. 1993;**212**:457–468.
50. Zambrano E, Barrios-de-Tomasi J, Cárdenas M, Ulloa-Aguirre A. Studies on the relative in-vitro biological potency of the naturally-occurring isoforms of intrapituitary follicle stimulating hormone. *Mol Hum Reprod*. 1996;**2**(8):563–571.
51. RRID:AB_2755044, https//scicrunch.org/resolver/AB_2755044.
52. Tranchant T, Durand G, Gauthier C, et al. Preferential β-arrestin signalling at low receptor density revealed by functional characterization of the human FSH receptor A189 V mutation. *Mol Cell Endocrinol*. 2011;**331**(1):109–118.
53. RRID AB_2814841, https//scicrunch.org/resolver/AB_2814841.
54. Lindau-Shepard B, Brumberg HA, Peterson AJ, Dias JA. Reversible immunoneutralization of human follitropin receptor. *J Reprod Immunol*. 2001;**49**(1):1–19.
55. RRID AB_10015289, https//scicrunch.org/resolver/AB_10015289.
56. Ulloa-Aguirre A, Dias JA, Bousfield G, Huhtaniemi I, Reiter E. Trafficking of the follitropin receptor. *Methods Enzymol*. 2013;**521**:17–45.
57. RRID AB_2107426, https//scicrunch.org/resolver/AB_2107426.
58. RRID AB_2797996, https//scicrunch.org/resolver/AB_2797996.
59. RRID:AB_2258681, https//scicrunch.org/resolver/AB_2258681.
60. RRID AB_772206, https//scicrunch.org/resolver/AB_772206.
61. Kara E, Crépieux P, Gauthier C, et al. A phosphorylation cluster of five serine and threonine residues in the C-terminus of the follicle-stimulating hormone receptor is important for desensitization but not for beta-arrestin-mediated ERK activation. *Mol Endocrinol*. 2006;**20**(11):3014–3026.
62. Wehbi V, Tranchant T, Durand G, et al. Partially deglycosylated equine LH preferentially activates beta-arrestin-dependent signaling at the follicle-stimulating hormone receptor. *Mol Endocrinol*. 2010;**24**(3):561–573.
63. RRID AB_331646, https//scicrunch.org/resolver/AB_331646.
64. RRID AB_2141292, https//scicrunch.org/resolver/AB_2141292.
65. Cassier E, Gallay N, Bourquard T, et al. Phosphorylation of beta-arrestin2 at Thr(383) by MEK underlies beta-arrestin-dependent activation of Erk1/2 by GPCRs. *Elife*. 2017; 6.
66. Heitzler D, Durand G, Gallay N, et al. Competing G protein-coupled receptor kinases balance G protein and β-arrestin signaling. *Mol Syst Biol*. 2012;**8**:590.
67. Landomiel F, De Pascali F, Raynaud P, et al. Biased signaling and allosteric modulation at the FSHR. *Front Endocrinol (Lausanne)*. 2019;**10**:148.
68. https://figshare.com/articles/Zarin_an_et_al_supplemental_Figs_S1-S4_pdf/10865987.
69. Luttrell LM, Wang J, Plouffe B, et al. Manifold roles of beta-arrestins in GPCR signaling elucidated with siRNA and CRISPR/Cas9. *Sci Signal*. 2018;**11**:1–22.
70. Thomas RM, Nechamen CA, Mazurkiewicz JE, Ulloa-Aguirre A, Dias JA. The adapter protein APPL1 links FSH receptor to inositol 1,4,5-trisphosphate production and is implicated in intracellular Ca(2+) mobilization. *Endocrinology*. 2011;**152**(4):1691–1701.
71. Lin YF, Tseng MJ, Hsu HL, Wu YW, Lee YH, Tsai YH. A novel follicle-stimulating hormone-induced G alpha h/phospholipase C-delta1 signaling pathway mediating rat sertoli cell Ca2+-influx. *Mol Endocrinol*. 2006;**20**(10):2514–2527.
72. Dahia CL, Rao AJ. Regulation of FSH receptor, PKIbeta, IL-6 and calcium mobilization: possible mediators of differential action of FSH. *Mol Cell Endocrinol*. 2006;**247**(1-2):73–81.
73. Flores JA, Leong DA, Veldhuis JD. Is the calcium signal induced by follicle-stimulating hormone in swine granulosa cells mediated by adenosine cyclic 3',5'-monophosphate-dependent protein kinase? *Endocrinology*. 1992;**130**(4):1862–1866.
74. Flores JA, Veldhuis JD, Leong DA. Follicle-stimulating hormone evokes an increase in intracellular free calcium ion concentrations in single ovarian (granulosa) cells. *Endocrinology*. 1990;**127**(6):3172–3179.
75. Sharma OP, Flores JA, Leong DA, Veldhuis JD. Cellular basis for follicle-stimulating hormone-stimulated calcium signaling in single rat Sertoli cells: possible dissociation from effects of adenosine 3',5'-monophosphate. *Endocrinology*. 1994;**134**(4):1915–1923.

76. Grasso P, Reichert LE Jr. Follicle-stimulating hormone receptor-mediated uptake of 45Ca2+ by proteoliposomes and cultured rat sertoli cells: evidence for involvement of voltage-activated and voltage-independent calcium channels. *Endocrinology.* 1989;**125**(6):3029–3036.
77. Grasso P, Reichert LE Jr. Follicle-stimulating hormone receptor-mediated uptake of 45Ca2+ by cultured rat Sertoli cells does not require activation of cholera toxin- or pertussis toxin-sensitive guanine nucleotide binding proteins or adenylate cyclase. *Endocrinology.* 1990;**127**(2):949–956.
78. Loss ES, Jacobus AP, Wassermann GF. Rapid signaling responses in Sertoli cell membranes induced by follicle stimulating hormone and testosterone: calcium inflow and electrophysiological changes. *Life Sci.* 2011;**89**(15-16):577–583.
79. Arey BJ, Stevis PE, Deecher DC, et al. Induction of promiscuous G protein coupling of the follicle-stimulating hormone (FSH) receptor: a novel mechanism for transducing pleiotropic actions of FSH isoforms. *Mol Endocrinol.* 1997;**11**(5):517–526.
80. Loreti N, Fresno C, Barrera D, et al. The glycan structure in recombinant human FSH affects endocrine activity and global gene expression in human granulosa cells. *Mol Cell Endocrinol.* 2013;**366**(1):68–80.
81. Donadeu FX, Ascoli M. The differential effects of the gonadotropin receptors on aromatase expression in primary cultures of immature rat granulosa cells are highly dependent on the density of receptors expressed and the activation of the inositol phosphate cascade. *Endocrinology.* 2005;**146**(9):3907–3916.
82. Combarnous Y, Guillou F, Martinat N. Comparison of in vitro follicle-stimulating hormone (FSH) activity of equine gonadotropins (luteinizing hormone, FSH, and chorionic gonadotropin) in male and female rats. *Endocrinology.* 1984;**115**(5):1821–1827.
83. Gordon WL, Bousfield GR, Ward DN. Comparative binding of FSH to chicken and rat testis. *J Endocrinol Invest.* 1989;**12**(6):383–392.
84. Crépieux P, Marion S, Martinat N, et al. The ERK-dependent signalling is stage-specifically modulated by FSH, during primary Sertoli cell maturation. *Oncogene.* 2001;**20**(34):4696–4709.
85. Wehbi V, Decourtye J, Piketty V, Durand G, Reiter E, Maurel MC. Selective modulation of follicle-stimulating hormone signaling pathways with enhancing equine chorionic gonadotropin/antibody immune complexes. *Endocrinology.* 2010;**151**(6):2788–2799.
86. Wang J, Hanada K, Staus DP, et al. Gαi is required for carvedilol-induced β1 adrenergic receptor β-arrestin biased signaling. *Nat Commun.* 2017;**8**(1):1706.
87. Gorczynska E, Handelsman DJ. The role of calcium in follicle-stimulating hormone signal transduction in Sertoli cells. *J Biol Chem.* 1991;**266**(35):23739–23744.
88. Thomas RM, Nechamen CA, Mazurkiewicz JE, Muda M, Palmer S, Dias JA. Follice-stimulating hormone receptor forms oligomers and shows evidence of carboxyl-terminal proteolytic processing. *Endocrinology.* 2007;**148**(5):1987–1995.
89. Suh PG, Park JI, Manzoli L, et al. Multiple roles of phosphoinositide-specific phospholipase C isozymes. *BMB Rep.* 2008;**41**(6):415–434.
90. Breen SM, Andric N, Ping T, et al. Ovulation involves the luteinizing hormone-dependent activation of G(q/11) in granulosa cells. *Mol Endocrinol.* 2013;**27**(9):1483–1491.
91. Gudermann T, Birnbaumer M, Birnbaumer L. Evidence for dual coupling of the murine luteinizing hormone receptor to adenylyl cyclase and phosphoinositide breakdown and Ca2+ mobilization. Studies with the cloned murine luteinizing hormone receptor expressed in L cells. *J Biol Chem.* 1992;**267**(7):4479–4488.
92. Gudermann T, Nichols C, Levy FO, Birnbaumer M, Birnbaumer L. Ca2+ mobilization by the LH receptor expressed in Xenopus oocytes independent of 3',5'-cyclic adenosine monophosphate formation: evidence for parallel activation of two signaling pathways. *Mol Endocrinol.* 1992;**6**(2):272–278.
93. Davis JS, Weakland LL, Farese RV, West LA. Luteinizing hormone increases inositol trisphosphate and cytosolic free Ca2+ in isolated bovine luteal cells. *J Biol Chem.* 1987;**262**(18):8515–8521.
94. Davis JS, Weakland LL, West LA, Farese RV. Luteinizing hormone stimulates the formation of inositol trisphosphate and cyclic AMP in rat granulosa cells. Evidence for phospholipase C generated second messengers in the action of luteinizing hormone. *Biochem J.* 1986;**238**(2):597–604.
95. Kleinau G, Worth CL, Kreuchwig A, et al. Structural-functional features of the thyrotropin receptor: a class A G-protein-coupled receptor at work. *Front Endocrinol (Lausanne).* 2017;**8**:86.
96. Reiter E, Ayoub MA, Pellissier LP, et al. β-arrestin signalling and bias in hormone-responsive GPCRs. *Mol Cell Endocrinol.* 2017;**449**:28–41.
97. Jiang X, Liu H, Chen X, et al. Structure of follicle-stimulating hormone in complex with the entire ectodomain of its receptor. *Proc Natl Acad Sci U S A.* 2012;**109**(31):12491–12496.

98. Timossi C, Damián-Matsumura P, Dominguez-González A, Ulloa-Aguirre A. A less acidic human follicle-stimulating hormone preparation induces tissue-type plasminogen activator enzyme activity earlier than a predominantly acidic analogue in phenobarbital-blocked pro-oestrous rats. *Mol Hum Reprod*. 1998;**4**(11):1032–1038.
99. Padmanabhan V, Lang LL, Sonstein J, Kelch RP, Beitins IZ. Modulation of serum follicle-stimulating hormone bioactivity and isoform distribution by estrogenic steroids in normal women and in gonadal dysgenesis. *J Clin Endocrinol Metab*. 1988;**67**(3):465–473.
100. Wide L, Bakos O. More basic forms of both human follicle-stimulating hormone and luteinizing hormone in serum at midcycle compared with the follicular or luteal phase. *J Clin Endocrinol Metab*. 1993;**76**(4):885–889.
101. Zambrano E, Olivares A, Mendez JP, et al. Dynamics of basal and gonadotropin-releasing hormone-releasable serum follicle-stimulating hormone charge isoform distribution throughout the human menstrual cycle. *J Clin Endocrinol Metab*. 1995;**80**(5):1647–1656.
102. Wide L, Eriksson K. Dynamic changes in glycosylation and glycan composition of serum FSH and LH during natural ovarian stimulation. *Ups J Med Sci*. 2013;**118**(3):153–164.
103. Wide L, Eriksson K. Low-glycosylated forms of both FSH and LH play major roles in the natural ovarian stimulation. *Ups J Med Sci*. 2018;**123**(2):100–108.
104. Mastrangeli R, Satwekar A, Cutillo F, Ciampolillo C, Palinsky W, Longobardi S. In-vivo biological activity and glycosylation analysis of a biosimilar recombinant human follicle-stimulating hormone product (Bemfola) compared with its reference medicinal product (GONAL-f). *Plos One*. 2017;**12**(9):e0184139.
105. RRID AB_2814868, https//scicrunch.org/resolver/AB_2814868.